Received March 26, 2018, accepted April 5, 2018, date of publication April 19, 2018, date of current version May 16, 2018.

Digital Object Identifier 10.1109/ACCESS.2018.2828609

A Procedure to Design Fault-Tolerant Wide-Area Damping Controllers

MURILO E. C. BENTO[1], (Student Member, IEEE), DANIEL DOTTA[2], (Member, IEEE), ROMAN KUIAVA[3], (Member, IEEE), AND RODRIGO A. RAMOS[1], (Senior Member, IEEE)

[1]University of São Paulo, São Carlos 13566-590, Brazil
[2]University of Campinas, Campinas 13083-852, Brazil
[3]Federal University of Paraná, Curitiba 80060-000, Brazil

Corresponding author: Murilo E. C. Bento (murilo.bento@usp.br)

This work was supported by FAPESP under Grant 2015/02569-6, Grant 2015/24245-8, Grant 2015/18806-7, and Grant 2016/08645-9.

ABSTRACT The idea of a smart grid is based on the increased integration of information technologies throughout the power grid. Technologies, such as phasor measurement units, are being deployed to increase the number of wide-area measurements across the bulk power system providing increased awareness of the system operational state. However, from a critical infrastructure perspective, the advanced metering infrastructure introduces a concern: the loss of communication among devices and the power grid. This communication loss may interfere with the wide-area control system performance and adversely affect the power system dynamics. This paper proposes a method based on genetic algorithms for wide-area robust damping controller design considering multiple operation points and loss of communication links related to the input and to the output of the central controller. The method is applied to enhance the damping of the electromechanical oscillations in an IEEE benchmark system: the simplified 14-generator model of the Southeastern Australian power system. The performance of the designed controller is evaluated using modal analysis and non-linear simulations in the time domain. The obtained results demonstrate the effectiveness of the method to design a single centralized controller that provides satisfactory damping to the electromechanical oscillations over several operating points, even when there is a loss of a communication link, thus being robust with respect to is an important aspect of a critical power grid infrastructure.

INDEX TERMS Machine learning, wide-area damping control, WAMS.

I. INTRODUCTION

A. MOTIVATION

Power system stability is essentially a single problem [1]. However, several phenomena may emerge after a critical fault or contingency making the analysis of power system stability as a single problem impracticable. Hence, power system stability studies are divided into different categories mainly based on the physical nature of the resulting forms of instability and the size of the disturbance considered. The low-frequency electromechanical oscillations ($0.2 - 2.0$ Hz) are one of the physical phenomena inherent to the interconnected power systems operation. These oscillations result from dynamic interactions between the various generators of a system, through its transmission network. Insufficient damping of these electromechanical oscillations is usually associated with the presence of Automatic Voltage Regulators (AVRs) with high gain in the generators and long transmission lines with weak connections between different areas of a system. The effects of oscillations must be minimized because they limit power transfers on transmission lines, induce stress in the mechanical shaft of generators as well as may lead to power system blackouts.

The Power System Stabilizers (PSSs) are the most cost-effective controls for damping electromechanical oscillations. Such device is installed in the generator excitation system using local generator speed or frequency measurement as a control input, which means that the PSSs are local and decentralized controllers. The PSS output acts through the generator's AVR introducing a component of electrical torque on the rotor which is in phase with speed deviations. The performance of the PSS design is evaluated by examining the closed loop power system eigenproperties by checking if the designed controller improved the damping of the electromechanical modes.

Remarkable research effort has been done to conceive robust design methods for tuning and coordination of PSSs.

However, the inclusion of distributed generation and transmission system expansion constraints as a result of environmental or economic restrictions are increasingly making local PSSs ineffective to deal with poorly damped oscillations. A practical example [2] is the western North American power system (wNAPS), where the primary damping controllers (local PSSs units) have limited effectiveness for inter-area modes. One of the proposed solutions is to improve the oscillations damping by using a control system with wide-area measurements.

The Wide-Area Measurement Systems (WAMS) represents a paradigm shift in power system monitoring. They allow the power system dynamic monitoring which is not possible with the traditional Supervisory Control and Data Acquisition (SCADA) and state-estimators. In spite of not being a new technology, recently the synchronized phasor measurement systems have been experimenting a significant expansion. This expansion is also verified by the number of phasor measurements units (PMUs) installed in large power systems such as USA and China [3], [4]. Regarding control applications, important research efforts for angular, voltage and frequency stability performance improvement are summarized in [5] and [6]. Among these applications, the Wide-Area Damping Control (WADC) was the one extensively explored in the literature. When implemented, a WADC becomes part of a critical infrastructure of the power grid, which can then be viewed in the context of smart grids, due to the centralized nature of the control structure and the communication infrastructure that must be built to enable this implementation.

B. LITERATURE REVIEW

Different control schemes and several control design techniques have been considered for wide-area oscillation damping. The first works were dedicated to showing the control effectiveness and tackle the adverse impact of fixed delay in communicating remote signals [7]–[9], time-variant delays were presented in [10]–[13] and low data rate/bandwidth availability was presented in [14]. Recently, an innovative model-free approach was proposed based on goal representation heuristic dynamic programming (GrHDP) algorithm [15] with adaptive delay compensation for WADC. This approach only needs input/output signals and do not need model information of the controlled plant and really represents an advance compared to previous works. However, the complete loss of communication channels is the relevant practical challenge of this control scheme. One of the proposed solutions for this problem was to consider redundant communication channels [16]–[18], however, this solution may increase the size of the controller and limit the number of signals that can be used in the controller. Recently, this issue also became more important because of the high integration of electrical and communication systems, which turns possible to access a large amount of real-time data. However, it makes the system more susceptible to security threats such as cyber attacks [19]–[24]. Even redundant communication links are vulnerable to cyber attacks which can make this type of control fail and reduce its performance.

The Fault-tolerant Control (FTC) techniques present potential to improve controller performance under failures in the communication channels [25], [26]. The fault-tolerant controller aims to guarantee a satisfactory performance for a given system under normal and fault conditions. Fault conditions can be understood as faults or failures in actuators, sensors or other control components. Fault-tolerant control systems can be classified as passive or active [27]. In the passive case, the controller is designed to be sufficiently robust to pre-specified faults so that no modification in the control process is needed after experiencing a fault. In the active case, some preliminary actions are first taken to detect and to diagnose the fault, and the controller is then reconfigured based on off-line or an online strategy. In [17], the authors use mathematical morphology to identify a communication failure, and then automatically switches to another redundant healthy communication route. In [28], the authors present a proposition to handle actuators faults by reconfiguring remain controls in power transmission system using synchrophasors. A fault tolerant virtual actuator is designed to stabilize the system following local control device failure. Although the authors' results show the ability of control reconfiguration to keep the stability, the application of the passive techniques is more promising for power system applications given that to detect, diagnose and design of a controller, for a large power system, is still considered to be infeasible for online applications task. The application of the passive fault-tolerant technique for wide-area damping control is introduced in [29] and [30]. These works propose a quasi-decentralized control scheme based on a supplementary power oscillation damping (POD) control of a static VAr compensator (SVC) to enhance damping of relevant inter-area oscillations. The proposed control design guarantee the system stability even though the remote signal is lost. The main drawback of the proposed control scheme is that the SVC location has a strong influence on the capacity of the controller in damping inter-area modes. The authors consider the variation of operating conditions in the control design by selecting an appropriate weighting function (H_∞) in the synthesis process. The case study also includes the test results of five different operating conditions. In both cases, an approach based on Linear Matrix Inequalities (LMIs) is used, where its major drawback is the presence of Lyapunov variables, which grow quadratically with the system size. As a result, current LMI solvers quickly break down when plants get sizeable.

The Genetic Algorithms (GA) may present an alternative approach for complex problems such as the Fault-Tolerant Passive Control (FTPC) design. These algorithms belong to the larger class of evolutionary algorithms, where search and optimization are based on the evolution mechanisms of the living beings. The application of GA methods for power system damping control can be found in [14] and [31]–[33]. The FTPC problem involves a lot of uncertainties such as operating conditions and sensibility of communication failures,

as well as, a high number of controller parameters to be tuned, which significantly contributes to the increase of the solution space size. All these aspects improve the control design complexity and justify the application of GA methods, once they can explore the solution space very efficiently and are therefore less likely to be trapped in a local minimum that does not correspond to a satisfactory solution. This is an advantage when compared to other traditional methods (LMI or Riccati) [34]. Notice that the GA methods are also simple to use what makes a significant difference for practical applications.

C. CONTRIBUTIONS

The main paper contributions are summarized as follows: *i)* a novel approach to design robust passive fault-tolerant fixed-order two-level damping controllers for power systems; *ii)* The proposed method can deal with high order power systems, without relying on modal reduction methods; *iii)* the approach also includes parametric uncertainties in the design with stability and performance guarantee resulting on low order robust controllers; *iv)* the method presents simple application, and it is not necessary to rely on weight filters selection (H_2 and H_∞), which certainly may increase the complexity of control design especially for large power systems. Additionally, this procedure is of practical application because it does not demand special knowledge in control theory and may be helpful for practical power system engineers; *v)* no redundant communication channels are necessary since the loss of one of them is considered in the design of the controller.

The paper is organized as follows. Section II presents the two-level control structure description. Section III presents the power system and controller model. Section IV presents the wide-area damping control method for central controllers. In section V, the performance of the proposed controllers is evaluated both through small signal stability analysis and non-linear time domain simulations. Finally, concluding remarks are given in Section VI.

II. CONTROL STRUCTURE DESCRIPTION

The two-level control can be described, as shown in Fig. 1, for two control layers. The first one, composed by AVR-PSS control scheme (block 'Generator Local Controllers' in Fig. 1) and generically illustrated in Fig. 2, is the decentralized control. In general, these local controllers are a property of the different utilities with different control design procedures. Notice that the decentralized control design is responsibility of the power system utilities and it will not be considered in this work. Therefore, the Independent System Operators (ISO) engineers cannot fastly retuning the local control without utility agreement. The utility agreement process may take considerable time.

Hence, in this paper the AVR-PSSs control schemes, as well as, the supplementary controllers for the FACTS devices are assumed to be already tuned and operating in the system, which means that only the design of the central controller is considered. But, it is important to point out that the proposed wide-area damping control method guarantees a coordinated action among the local controllers and the central control to improve the damping performance of the power system, once the power system model adopted for the central control design takes into account the AVR-PSSs and FACTS devices models.

The main advantage of the central controller is that it allows a much more effective optimization of the global performance of the power system. This controller is located in the control center close or as a function embedded in the PDC (Phasor Data Concentrator) and its design is carried out on top of the decentralized control. It is faster and easier retunning this controller when compared with decentralized control.

In this particular situation, the FTPC design must be robust to several operating conditions (which are combinations of different network topologies, load levels, generation schedules and others), as well as, sensors and actuators communication channels failures. This may reduce the necessity of control redesign required by previous approaches such as presented in [16]. The main outcome is a controller that preserves an acceptable performance even under communication channels failures. These advantages improve control effectiveness and the potential to be applied in the real power systems.

III. THE CONTROL PROBLEM FORMULATION

The first part of this section presents the model for the controlled system, as illustrated in Fig. 1, which is used to design the centralized controller. The structure proposed for the centralized controller is described in subsection III-B. The closed loop system and the control problem statement are presented in subsections III-C and III-D, respectively.

A. CONTROLLED SYSTEM

The controlled system comprehends the power system with decentralized controllers, sensors (PMUs) and communication channels. The decentralized controllers (that is, the local controllers) are represented by the AVR-PSS control structure following IEEE standard types [35]. The main issue related with the PMUs (the delay in phasor acquisition and estimation is not significant) is the transmission delay in the communication channel. In this paper, the transmission delay is considered fixed in all communication channels (block 'Delay' in Fig. 1) and can be modeled by the traditional second order Padé approximation in cascade connection with the open loop system. However, the traditional Padé approximation with proper second order function presents a pulse at t=0 for step-response in time-domain. In [36], a variation of Padé approximation is proposed to minimize this effect keeping the frequency domain proprieties. The proposed transfer function is given by

$$G_d(s) = \frac{6 - 2Ts}{6 + 4Ts + (sT)^2} \tag{1}$$

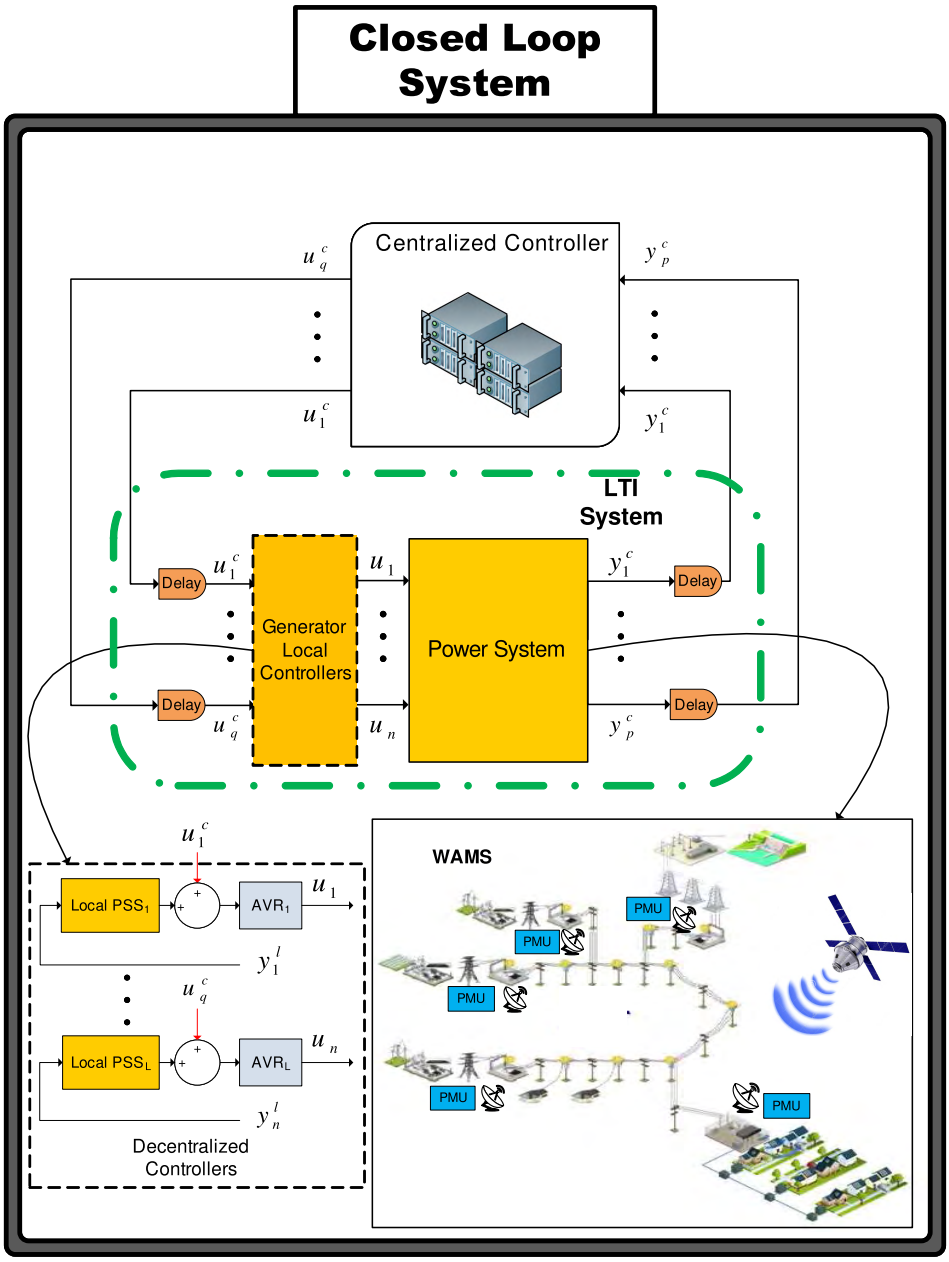

FIGURE 1. FTC Control Structure.

where T is the delay time. The transfer function (1) is converted in the state-space form and then incorporated to the controlled system model. For more informations about this modeling step, see [34].

The controlled system can be modeled by a set of nonlinear differential algebraic equations (DAE) model. These equations can be generically defined by:

$$\dot{\hat{\mathbf{x}}} = f(\hat{\mathbf{x}}, \mathbf{z}, \hat{\mathbf{u}}) \tag{2}$$

$$0 = g(\hat{\mathbf{x}}, \mathbf{z}) \tag{3}$$

$$\hat{\mathbf{y}} = h(\hat{\mathbf{x}}, \mathbf{z}) \tag{4}$$

where $\hat{\mathbf{x}} \in \mathbb{R}^n$, $\mathbf{z} \in \mathbb{R}^m$, $\hat{\mathbf{u}} \in \mathbb{R}^p$ and $\hat{\mathbf{y}} \in \mathbb{R}^q$ are, respectively, the vectors with the state variables (ex., generator internal angles and speeds), the algebraic variables (ex., static load voltages and angles), controllable variables (ex., AVR setpoints) and the system outputs (ex., the generator speeds).

The nonlinear equations (2)-(4) can be linearized around a nominal operating point and represented by:

$$\dot{\mathbf{x}} = \mathbf{J_1}\mathbf{x} + \mathbf{J_2}\mathbf{z} + \mathbf{B}\mathbf{u} \tag{5}$$

$$0 = \mathbf{J_3}\mathbf{x} + \mathbf{J_4}\mathbf{z} \tag{6}$$

$$\mathbf{y} = \mathbf{C_1}\mathbf{x} + \mathbf{C_2}\mathbf{z} \tag{7}$$

where $\mathbf{J_1}$ and $\mathbf{J_2}$ ($\mathbf{J_3}$ and $\mathbf{J_4}$) are the Jacobian matrices of $f(\hat{\mathbf{x}}, \mathbf{z}, \hat{\mathbf{u}})$ and $g(\hat{\mathbf{x}}, \mathbf{z})$ with respect to the state and the algebraic variables, respectively. By eliminating the algebraic variables from the model (5)-(7), it is possible to obtain the following

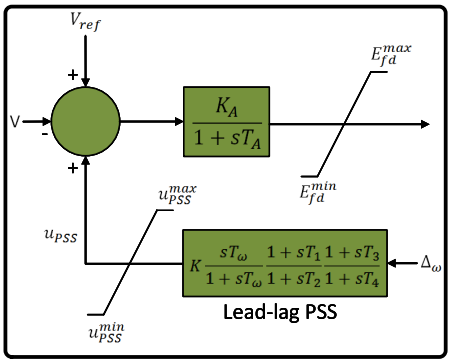

FIGURE 2. Generic AVR-PSS control scheme.

representation in state-space for the controlled system:

$$\dot{\mathbf{x}} = \mathbf{A}\mathbf{x} + \mathbf{B}\mathbf{u} \tag{8}$$

$$\mathbf{y} = \mathbf{C}\mathbf{x} \tag{9}$$

where $\mathbf{A} = \mathbf{J_1} - \mathbf{J_2}\mathbf{J_4^{-1}}\mathbf{J_3}$ corresponds to the system state matrix and $\mathbf{C} = \mathbf{C_1} - \mathbf{C_2}\mathbf{J_4^{-1}}\mathbf{J_3}$ corresponds to the output matrix. Also, $\mathbf{x}$, $\mathbf{u}$ and $\mathbf{y}$ represent the deviation of the state variables ($\hat{\mathbf{x}}$), the controlled variables ($\hat{\mathbf{u}}$) and the system outputs ($\hat{\mathbf{y}}$), respectively, with respect to the equilibrium point adopted for the linearization process.

B. THE CENTRALIZED CONTROLLER STRUCTURE

The structure of the centralized controller is modeled by a transfer function matrix given by

$$\mathbf{CC}(s) = \begin{bmatrix} cc_{11}(s) & \dots & cc_{1q}(s) \\ cc_{21}(s) & \dots & cc_{2q}(s) \\ \vdots & \ddots & \vdots \\ cc_{p1}(s) & \dots & cc_{pq}(s) \end{bmatrix} \tag{10}$$

The transfer functions $cc_{ij}(s)$, $i = 1, \cdots, p, j = 1, \cdots, q$ are based on decentralized PSS model generally described by second order linear transfer functions [37]. In this paper, the function $cc_{ij}(s)$ is limited to second order avoiding large control structures that cannot be implemented in practice. The function $cc_{ij}(s)$ is given by:

$$cc_{ij}(s) = \frac{b_{ij}^1 s + b_{ij}^0}{s^2 + a^1 s + a^0} + d_{ij} \tag{11}$$

In this paper, the transfer function (10) is represented by the canonical observable realization. Notice that there are no constraints related to transfer function representation. The canonical controllable realization can also be used. The state-space observable realization is given as follows.

$$\dot{\mathbf{x}}_c = \mathbf{A}_c\,\mathbf{x}_c + \mathbf{B}_c\,\mathbf{y} \tag{12}$$

$$\mathbf{u} = \mathbf{C}_c\,\mathbf{x}_c + \mathbf{D}_c\,\mathbf{y} \tag{13}$$

where $\mathbf{x_c}$ is the controller state vector and matrices $\mathbf{A}_c$, $\mathbf{B}_c$, $\mathbf{C}_c$ and $\mathbf{D}_c$ are given by

$$\mathbf{A}_c = \begin{bmatrix} \mathbf{A}_1 & 0 & \dots & 0 \\ 0 & \mathbf{A}_2 & \dots & 0 \\ \vdots & \vdots & \ddots & \vdots \\ 0 & 0 & \dots & \mathbf{A}_p \end{bmatrix}, \quad \mathbf{A}_i = \begin{bmatrix} 0 & -a^0 \\ 1 & -a^1 \end{bmatrix}$$

for $i = 1, \dots, p$,

$$\mathbf{B}_c = \begin{bmatrix} \mathbf{B}_1 \\ \mathbf{B}_2 \\ \vdots \\ \mathbf{B}_p \end{bmatrix}, \quad \mathbf{B}_i = \begin{bmatrix} b_{i1}^0 & b_{i2}^0 & \dots & b_{iq}^0 \\ b_{i1}^1 & b_{i2}^1 & \dots & b_{iq}^1 \end{bmatrix}$$

for $i = 1 \dots p$,

$$\mathbf{C}_c = \begin{bmatrix} \mathbf{C}_1 & \mathbf{C}_2 & \dots & \mathbf{C}_p \end{bmatrix}, \quad \mathbf{C}_i = \begin{bmatrix} 0 \\ \vdots\ e_i \\ 0 \end{bmatrix}$$

for $i = 1, \dots, p$ and e_i is the i^{th} column of the identity matrix $\mathbf{I}_q$.

$$\mathbf{D}_c = \begin{bmatrix} \mathbf{d}_{11} & \mathbf{d}_{12} & \dots & \mathbf{d}_{1q} \\ \mathbf{d}_{21} & \mathbf{d}_{22} & \dots & \mathbf{d}_{2q} \\ \vdots & \vdots & \ddots & \vdots \\ \mathbf{d}_{p1} & \mathbf{d}_{p2} & \dots & \mathbf{d}_{pq} \end{bmatrix},$$

C. CLOSED-LOOP SYSTEM

The closed-loop system is given by the connection of the centralized controller to the controlled system, as shown in Fig. 1. Using (8)-(9) to represent the power system with time delays and including the centralized controller given by (12)-(13), the closed-loop system can be represented by

$$\dot{\mathbf{x}}_{cl} = \mathbf{A_{cl}}\mathbf{x_{cl}} \tag{14}$$

where $\mathbf{x_{cl}} = \begin{bmatrix} \mathbf{x}\ \mathbf{x_c} \end{bmatrix}^{\mathbf{T}}$ is the augmented state vector and $\mathbf{A_{cl}}$ is given by

$$\mathbf{A_{cl}} = \begin{bmatrix} \mathbf{A} + \mathbf{B}\mathbf{D_c}\mathbf{C} & \mathbf{B}\mathbf{C_c} \\ \mathbf{B_c}\mathbf{C} & \mathbf{A_c} \end{bmatrix} \tag{15}$$

D. DESIGN REQUIREMENTS AND THE CONTROL PROBLEM STATEMENT

The design requirements that must be fulfilled by the FTC passive wide-area damping controller are: robustness for multiple operating points and faults in sensor and/or actuators.

The loss of simultaneous communication channels may not impair the controller performance, however, there is no formal guarantee of stability for this case and the central controller should be shut down or a new control design should be realized. On the other hand, it should be noted the main advantage from hierarchical controllers is that they can keep the power system operating using the first level control (decentralized controllers). The central controller main goal is to optimize the operation of the decentralized controllers and not substitute them. In this work, we adopted a deterministic reliability criterion (N-1) largely used in power system

planning to design the central controller. However, more than one communication loss can be considered with a new set of additional combinations in the control problem formulation. The robustness for multiple operating points includes load variation and transmission lines contingencies. These changes only affect the matrix $\mathbf{A}$, then for the l-th operating point, the state matrix[1] is given by $\mathbf{A^l}$.

The sensor and actuator faults are considered in the control problem formulation, respectively, by input and output communication channel losses, which affect the size of matrices $\mathbf{B}$ and $\mathbf{C}$ of the controlled system and, consequently, the size of matrices $\mathbf{B_c}$, $\mathbf{C_c}$ and $\mathbf{D_c}$ of the centralized controller. For example, for the case where the i-th input communication channel is lost, the i-th row of $\mathbf{C}$ is eliminated, as well as, the i-th column of matrices $\mathbf{B_c}$ and $\mathbf{D_c}$. A similar analysis can be done for the case where an output communication channel is lost. The main reason for performing this change on the matrices size is to avoid the presence of low-rank matrices during the search process. In this work, the loss of only one communication channel at a time (input-output) is considered. In practice, if two or more channels are simultaneously lost, then the centralized controller must be switched off. Due to resizing process, three categories can be defined based on closed-loop augmented system size. They are described as follows:

- All communication channels up

$$\mathbf{A_{cl}^l} = \begin{bmatrix} \mathbf{A^l} + \mathbf{B}\mathbf{D_c}\mathbf{C} & \mathbf{B}\mathbf{C_c} \\ \mathbf{B_c}\mathbf{C} & \mathbf{A_c} \end{bmatrix} \tag{16}$$

  where $l = 1, \ldots, L$, being L the number of operating points considered in the control design.
- Failure of central controller input communication channel

$$\mathbf{A_{cl}^{l,s}} = \begin{bmatrix} \mathbf{A^l} + \mathbf{B}\mathbf{D_c}^s\mathbf{C}^s & \mathbf{B}\mathbf{C_c} \\ \mathbf{B_c}^s\mathbf{C}^s & \mathbf{A_c} \end{bmatrix} \tag{17}$$

  where $l = 1, \ldots, L$ and $s = 1, \ldots, p$, being p the number of possible combinations of failure at controller input.
- Failure of central controller output communication channel

$$\mathbf{A_{cl}^{l,t}} = \begin{bmatrix} \mathbf{A^l} + \mathbf{B}^t\mathbf{D_c}^t\mathbf{C} & \mathbf{B}^t\mathbf{C_c}^t \\ \mathbf{B_c}\mathbf{C} & \mathbf{A_c} \end{bmatrix} \tag{18}$$

  where $l = 1, \ldots, L$ and $t = 1, \ldots, q$, being q the number of possible combinations of failure at controller output.

The control problem is then to determine the matrices $\mathbf{A_c}$, $\mathbf{B_c}$ and $\mathbf{D_c}$ of the centralized controller that fulfills some desired closed loop performance. This paper adopts the performance criterion that is most widely accepted by the industry, which states that the performance of the closed loop system can be considered as satisfactory if all eigenvalues of all closed-loop matrices (16)-(18) present a damping ratio greater than a minimum value equal to 5% [38].

[1]Notice that the matrix $\mathbf{A^l}$ is obtained from the linearization of the nonlinear model (2)-(4) with respect to the l-th operating point.

IV. WIDE-AREA DAMPING CONTROL METHOD

A. SEARCH PROBLEM FORMULATION

The GA objective function ($F()$) looks for a minimum damping ratio for all eigenvalues of all closed loop matrices considered in the control design, Eq. (19). The matrix $\mathbf{C_c}$ is fixed at an observable canonical form. The algorithm searches for the $\mathbf{A_c}$, $\mathbf{B_c}$ and $\mathbf{D_c}$ matrices that meet the control design requirements for the closed loop control system.

$$\mathbf{F}(\mathbf{A_{ck}},\mathbf{B_{ck}},\mathbf{D_{ck}}) = \zeta_{min}\begin{pmatrix} \mathbf{A^l} + \mathbf{B}\mathbf{D_{ck}}\mathbf{C} & \mathbf{B}\mathbf{C_c} \\ \mathbf{B_{ck}}\mathbf{C} & \mathbf{A_{ck}} \end{pmatrix} \tag{19}$$

for $k = 1, \ldots, P$, where P represents the population size.

The loss of signal in the controller input involves resizing matrices $\mathbf{B_c}$, $\mathbf{C}$ and $\mathbf{D_c}$ and the loss of output signal involves resizing matrices $\mathbf{B}$, $\mathbf{C_c}$ and $\mathbf{D_c}$. The objective function (19) must be modified in order to include robustness to loss of communications channels resulting in

$$\mathbf{F}(\mathbf{A_{ck}},\mathbf{B_{ck}},\mathbf{D_{ck}}) = \zeta^*_{min}\begin{Bmatrix} \zeta^1_{min}\begin{pmatrix} \mathbf{A^l} + \mathbf{B}\mathbf{D_{ck}}\mathbf{C} & \mathbf{B}\mathbf{C_c} \\ \mathbf{B_{ck}}\mathbf{C} & \mathbf{A_{ck}} \end{pmatrix} \\ \zeta^2_{min}\begin{pmatrix} \mathbf{A^l} + \mathbf{B}\mathbf{D_{c_k}}^s\mathbf{C}^s & \mathbf{B}\mathbf{C_c} \\ \mathbf{B_{c_k}}^s\mathbf{C}^s & \mathbf{A_{ck}} \end{pmatrix} \\ \zeta^3_{min}\begin{pmatrix} \mathbf{A^l} + \mathbf{B}^t\mathbf{D_{c_k}}^t\mathbf{C} & \mathbf{B}^t\mathbf{C_c}^t \\ \mathbf{B_{ck}}\mathbf{C} & \mathbf{A_{ck}} \end{pmatrix} \end{Bmatrix} \tag{20}$$

for $l = 1, \ldots, L$, $k = 1, \ldots, P$, $s = 1, \ldots, q$ and $t = 1, \ldots, p$.

Given a candidate solution $\mathbf{A_{ck}}, \mathbf{B_{ck}}, \mathbf{D_{ck}}$, the functions $\zeta^1_{min}()$, $\zeta^2_{min}()$ and $\zeta^3_{min}()$ estimates the minimum damping for no communication channels faults, sensors failures and actuators failures, respectively. These three functions are processed by the GA method and in the last step $\zeta^*_{min}()$ function estimates the lowest minimum damping among all of them.

Based on the definition above, the search problem may be formulated as

$$\max F(\zeta^*_{l,s,t}) \tag{21}$$

subject to,

$$\begin{aligned} a_{min} \le a^{ck}_{ij} \le a_{max} \quad & \forall\, i \in \mathbb{N}^{2p}, j \in \mathbb{N}^{2p} \\ b_{min} \le b^{ck}_{ij} \le b_{max} \quad & \forall\, i \in \mathbb{N}^{p}, j \in \mathbb{N}^{q} \\ d_{min} \le d^{ck}_{ij} \le d_{max} \quad & \forall\, i \in \mathbb{N}^{p}, j \in \mathbb{N}^{q} \end{aligned} \tag{22}$$

where $a^{ck}_{ij} \in \mathbb{C}$, $b^{ck}_{ij} \in \mathbb{R}$ and $d^{ck}_{ij} \in \mathbb{R}$ are the elements of the matrices $\mathbf{A_{ck}}$, $\mathbf{B_{ck}}$ and $\mathbf{D_{ck}}$, respectively. The matrix $\mathbf{A_{ck}}$ elements are limited in order to improve the system performance, simple controller development and to save computational time in control design. Regarding system performance, the proposed controller must be stable (negative poles) as well as limited to the electromechanical modes frequency range in a way to improve the phase margin gain in this respective region. One of the consequences of an unstable compensator is that closed-loop system is only conditionally stable. Additionally, a limited range of these elements helps the GA method to find out the poles of the controller reducing the

computational burden. The limits of the matrices $\mathbf{B_{ck}}$ and $\mathbf{D_{ck}}$ are limited to avoid high control effort what can impair the controller performance in nonlinear systems.

B. GENETIC OPERATORS

The selection was performed by an elitist strategy. The best individual, represented by matrices $(\mathbf{A_{ck}}, \mathbf{B_{ck}}, \mathbf{D_{ck}})$, of the current population is guaranteed to be in the subsequent population replacing the worse ones.

The crossover process consists to combine two individuals $(\mathbf{B_{ck}}, \mathbf{B_{ck+1}})$ and $(\mathbf{D_{ck}}, \mathbf{D_{ck+1}})$ exchanging rows randomly creating two new individuals $(2P)$ represented by $(\mathbf{A_{ck}}, \mathbf{B^*_{ck}}, \mathbf{D^*_{ck}})$ and $(\mathbf{A_{ck+1}}, \mathbf{B^*_{ck+1}}, \mathbf{D^*_{ck+1}})$. The mutation process chooses P individuals based on closed-loop damping estimation. A certain probability μ randomly generates a new line for $\mathbf{B^*_{ck}}$, new value for $\mathbf{D^*_{ck}}$ and new poles to form $\mathbf{A_{ck}}$. In short, at the end of each generation there are $2P$ individuals and only P, which maximizes the closed-loop system damping, are chosen for next generation.

C. INITIALIZATION AND STOP RULE

The initialization process is random but limited to a chosen sampling interval. The poles from matrix $\mathbf{A_{ck}}$ are chosen in a interval (a_{min}, a_{max}) as well as the matrices $\mathbf{B_{ck}}$ and $\mathbf{D_{ck}}$ elements are chosen in a interval (b_{min}, b_{max}) and (d_{min}, d_{max}) respectively for all individuals $(k = 1, \ldots, P)$.

The algorithm stops when the maximum number of generations is reached and the best individual is chosen to be the central controller. A reduced process of the algorithm is presented in section IV-D.

D. ALGORITHM

Step 1: Define the controller order, the number of generations (GN), the population size (P) and the number of operating points (L).

Step 2: Initialize the individuals $(\mathbf{A_{ck}}, \mathbf{B_{ck}}, \mathbf{D_{ck}}, k = 1, \ldots, P)$, calculate $F(\mathbf{A_{ck}}, \mathbf{B_{ck}}, \mathbf{D_{ck}})$, equation (20), for $k = 1, \ldots, P$, evaluate the individuals in decreasing order of damping and make $n_{GN} = 1$.

Step 3: In the crossover process, the P individuals will create new P ones with new genes (change $\mathbf{B_{ck}}$ rows and $\mathbf{D_{ck}}$ values). Arrange the $2P$ individuals by the decreasing damping value.

Step 4: In the mutation process, select the P worse individuals and create new P ones with new genes (change $\mathbf{B_{ck}}$ rows, $\mathbf{D_{ck}}$ values and $\mathbf{A_{ck}}$ poles). Arrange the $2P$ individuals by the decreasing damping value and select the P best ones

Step 5: If $n_{GN} = GN$, stops the algorithm; if not, $n_{GN} = n_{GN} + 1$ and go to the Step 3.

Step 6: The final controller is defined by $(\mathbf{A^*_c}, \mathbf{B^*_c}, \mathbf{D^*_c}) = (\mathbf{A_{c1}}, \mathbf{B_{c1}}, \mathbf{D_{c1}})$, the best solution.

V. APPLICATION RESULTS

The performance of the proposed method is assessed through its application to the Simplified 14-Generator Model of the Southeastern Australian Power System [39], [40], shown in the Fig. 3. It is one of IEEE standard benchmark models for the analysis and control of small-signal oscillatory dynamics in power systems. Specifically, this system is constituted by 14 generators, five Static VAR Compensators (SVCs), 59 buses and 104 lines with voltage levels ranging from 15 kV to 500 kV and six operating cases present in [39]. The synchronous generators are represented by fifth and sixth-order models. Three IEEE standard types of excitation systems are employed. They are: ST5B, AC4A and AC1A [35]. The SVC is represented as a perturbation in the shunt susceptance connected to the bus. The state-space model order is 174.

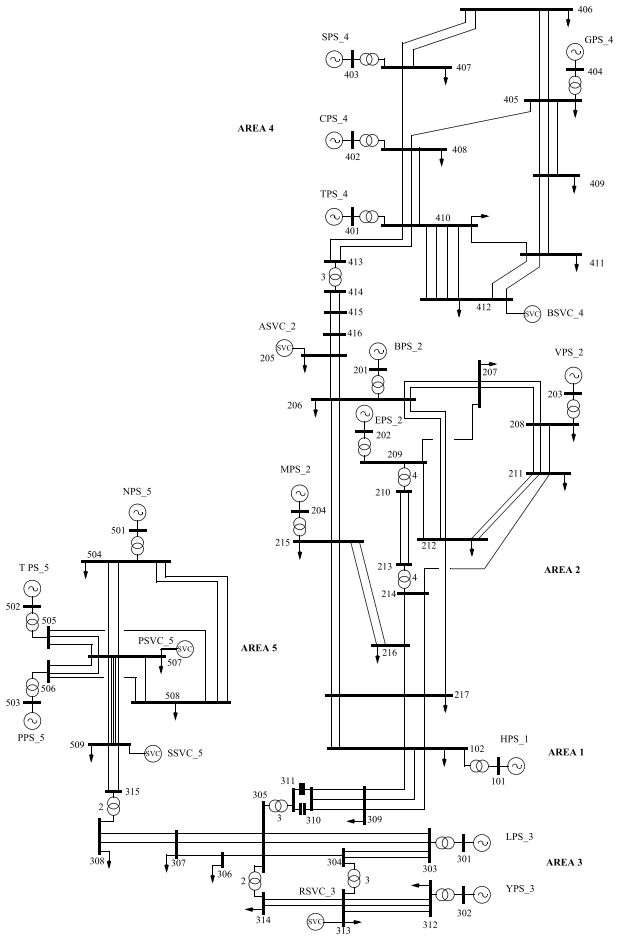

FIGURE 3. Simplified 14-generator model of the southeastern australian power system.

The system has been divided into five areas and there are three inter-area modes and ten local-area modes for the six operating cases present in [39] and [40]. Without PSSs, most of the electromechanical modes are unstable. For this reason, 14 PSSs were designed, one for each generator. The dominant oscillation mode for each of the six operating cases is presented in the Table 1. The dominant oscillation mode is considered as being the electromechanical mode that exhibits the lowest damping ratio among all the electromechanical modes. As it can be seen in Table 1, the modes for all the six operating conditions present damping ratios greater than 5%, thus fulfilling the adopted performance criterion.

TABLE 1. System dominant oscillation modes.

Operating case	Frequency (Hz)	Damping (%)
1	0.38	15.83
2	0.41	17.30
3	1.79	16.74
4	0.53	17.00
5	0.46	15.61
6	0.53	17.20

However, under topological changes, the system damping can decrease strongly, even with the presence of local PSSs. For instance, some severe contingencies are described as follows:

- Transmission line 207-209 is being serviced and a permanent three-phase fault occurred in the transmission line 209-212 (contingency C1) for the six operating cases.
- Transmission line 214-216 is being serviced and a permanent three-phase fault occurred in the transmission line 214-217 (contingency C2) for the six operating cases.
- Transmission line 206-212 is being serviced and a permanent three-phase fault occurred in the transmission line 215-216 (contingency C3) for the six operating cases.

TABLE 2. System dominant oscillation modes for the contingencies C1 to C3.

Contingency	Operating case	Frequency (Hz)	Damping (%)
C1	Worst of 6	1.23	-2.44
C2	Worst of 6	1.25	3.35
C3	Worst of 6	1.26	5.47

These permanent disconnections cause the emergence of a poorly damped oscillation mode, as shown in Table 2. Each row of this table presents the dominant oscillation mode with the lowest damping ration among the six operating conditions for each of the contingencies C1 to C3. These results confirm a poor damping performance operation. A central controller design is suitable to quickly restore the power system damping performance. Next subsection discusses the design of this controller via classical methods, which will be adopted as a basis of comparison with the one designed by the proposed methodology.

A. THE BASIS OF COMPARISON: A CENTRALIZED CONTROLLER DESIGNED BY CLASSICAL METHOD

Several methods are proposed in the literature for PSS tuning and coordination [41]–[44]. Although there are several excellent methods proposed in the literature, arbitrarily choosing one of them to be used as a basis of comparison in this paper is questionable because it neglects all others.

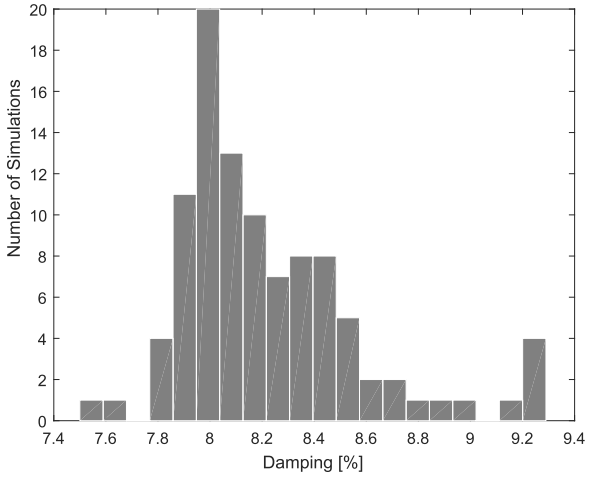

FIGURE 4. Histogram of minimum damping for 100 executions.

The conventional PSS, based on a lead-lag compensation structure [45], have been adopted by most utility companies mainly because of its simple structure and easy implementation [42]. This practical method was chosen as a basis of comparison with GA method. The practical process is to design a regular lead-lag compensator, described in [45] and [46], to provide appropriate compensation to the phase lag among different remote locations. The resulting central controller is presented in (26).

It should be noted that this method does not support robustness to the loss of communication channels. Thus, the unstable operating case described in (Table 2, row 1) was chosen as a base case.

B. THE PROPOSED APPROACH: TWO-LEVEL CONTROL DESIGN BY GA

A fault-tolerant WADC was designed. The damping controller must be robust for eighteen operation points (three contingencies for six available cases). For larger size power systems a model reduction method can be used to increase the method convergence speed. The best input-output signal pairs employing controllability and observability were selected for the three electromechanical modes presented in Table 2. The centralized level is formed by a controller with five inputs (the generators speeds) and five outputs. In a real phasor measurement system, the input signals could be bus frequencies or angles. Generator rotor angles and speeds can also be estimated from phasor measurement signals.

The following generators were selected to provide the inputs to the centralized controller: 101, 201, 302, 401 and 501. Times delays fixed in 200 ms were considered in the input and the output of the system model. As a result, five possible combinations of communication channels losses on the input of the central controller and five combinations on its output were taken into account in the control design. Hence, considering all the combinations among the 6 operating cases, 3 contingencies, and the possible output/input

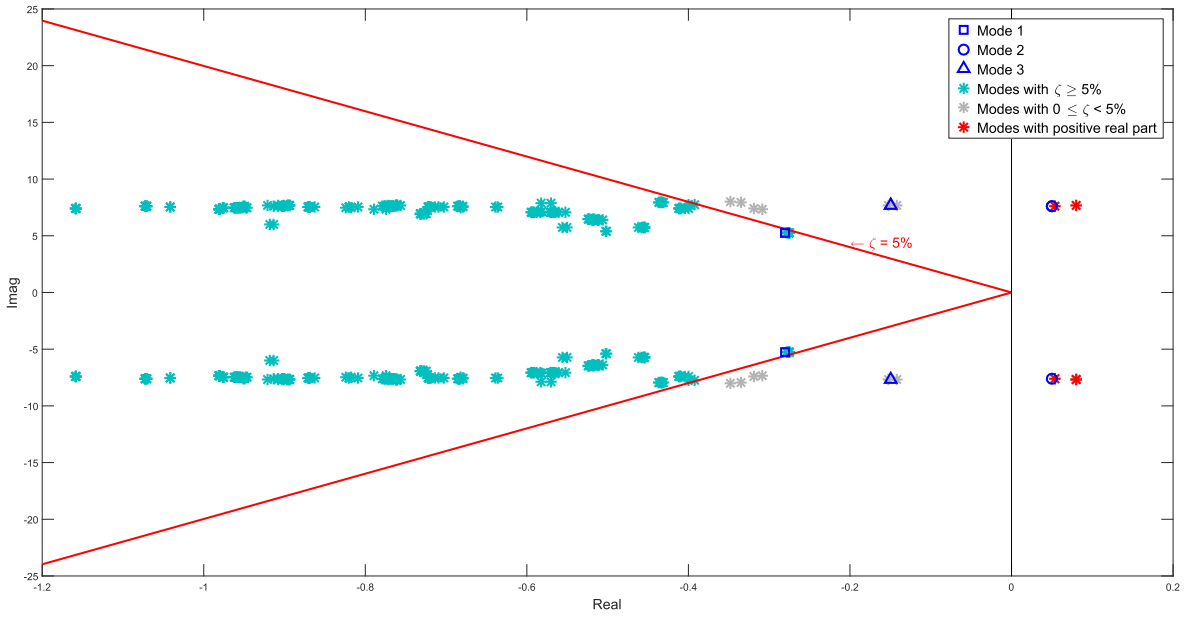

FIGURE 5. Dominant eigenvalues for the closed loop system with WADC-CM.

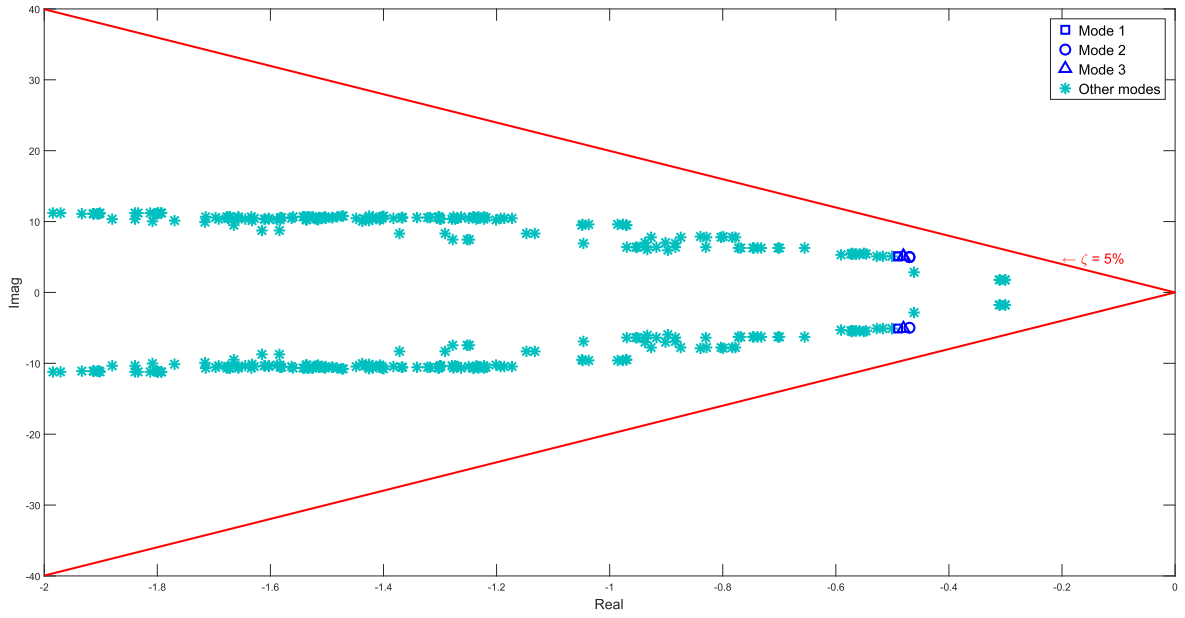

FIGURE 6. Dominant eigenvalues for the closed loop system with WADC-GA .

communication channels losses, a number of 198 different scenarios (or closed loop systems) were adopted for the design of the fault-tolerant WADC via the proposed GA method.

C. PERFORMANCE OF INITIALIZATION PROCESS

The initialization process is a key point for genetic algorithms because it can affect the convergence speed and also the quality of the final solution. The following test was conducted to evaluate the initialization process: 100 simulations were realized considering 1000 number of generations ($GN = 1000$) and a population size of 20 ($P = 20$) resulting in 100 controllers. Besides, $a_{min} = -0.1$, $a_{max} = -15$, $b_{min} = -1000$, $b_{max} = 1000$, $d_{min} = -100$ and $d_{max} = 100$. All operating points and possible communication channel losses were included in this test.

The simulation results are shown in histogram presented in Fig 4. The average minimum damping was 8.22% with standard deviation of 0.35%. All of 100 designed fault-tolerant WADC archived the safety margin of 5% minimum damping performance. The controller that provides the

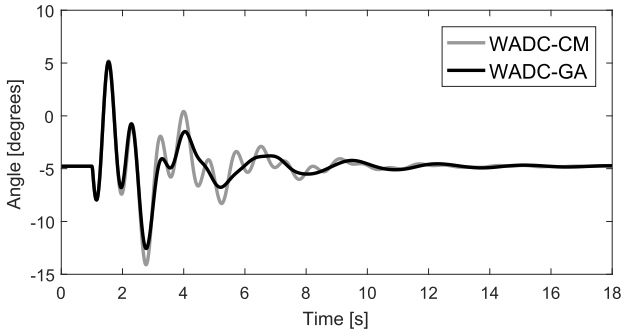

(a)

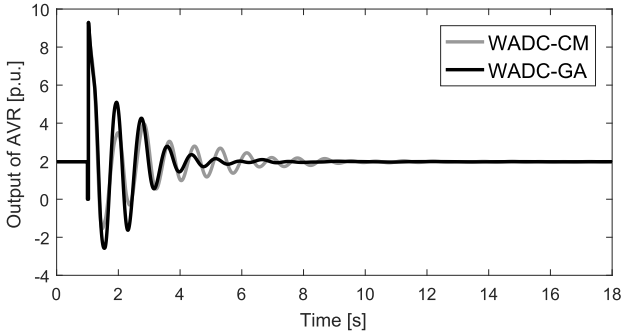

(b)

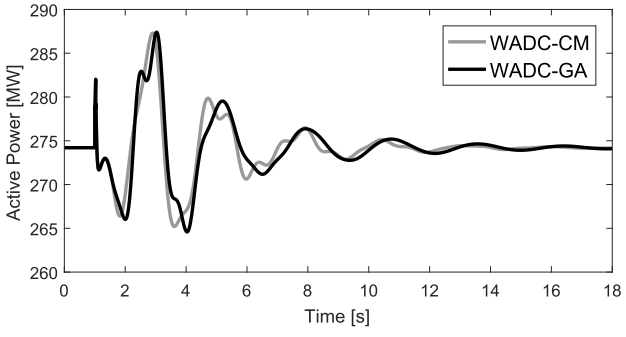

(c)

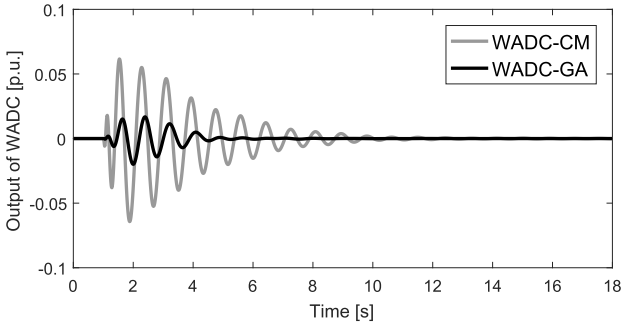

(d)

FIGURE 7. Nonlinear simulations for normal operating condition for the worst of C1 case. (a) Angle of the generator 101. (b) Output signal of the AVR of the generator 101. (c) Active power flow in line 506 - 507. (d) Output signal of the WADC for the generator 101.

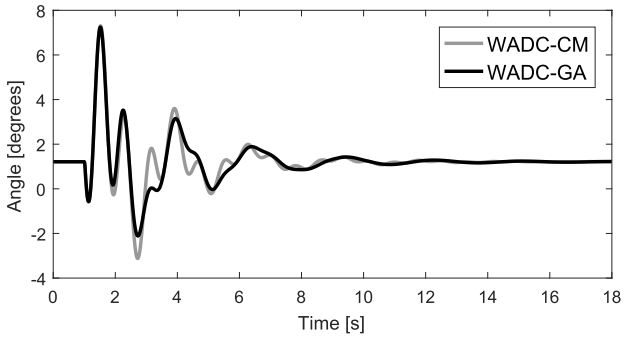

(a)

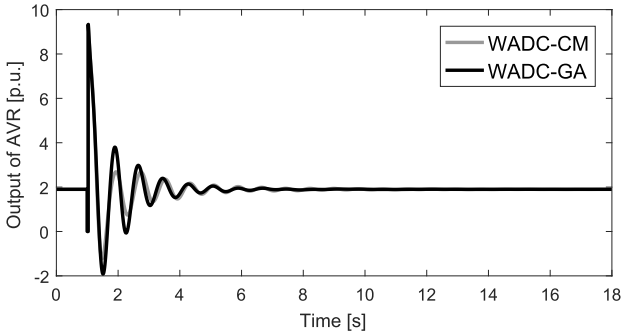

(b)

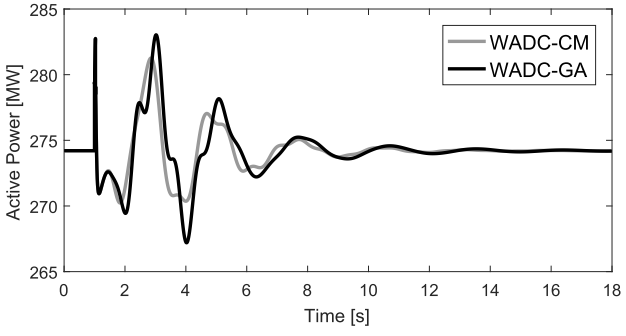

(c)

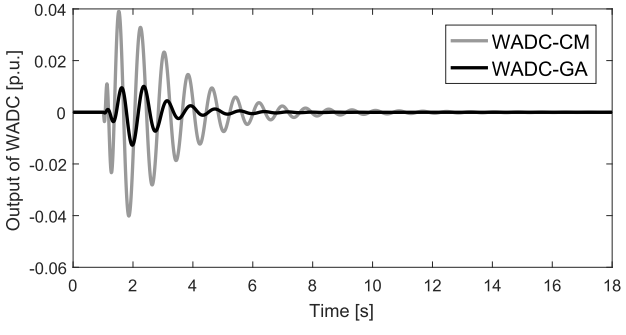

(d)

FIGURE 8. Nonlinear simulations for normal operating condition for the worst of C2 case. (a) Angle of the generator 101. (b) Output signal of the AVR of the generator 101. (c) Active power flow in line 506 - 507. (d) Output signal of the WADC for the generator 101.

highest closed loop system damping was chosen for modal analysis and time-domain non-linear simulations.

The fault-tolerant WADC which provided the highest minimum damping was chosen and resulting transfer function is presented in (25).

D. MODAL ANALYSIS

The small-signal stability analysis is performed to evaluate the controller performance. The classic controller was

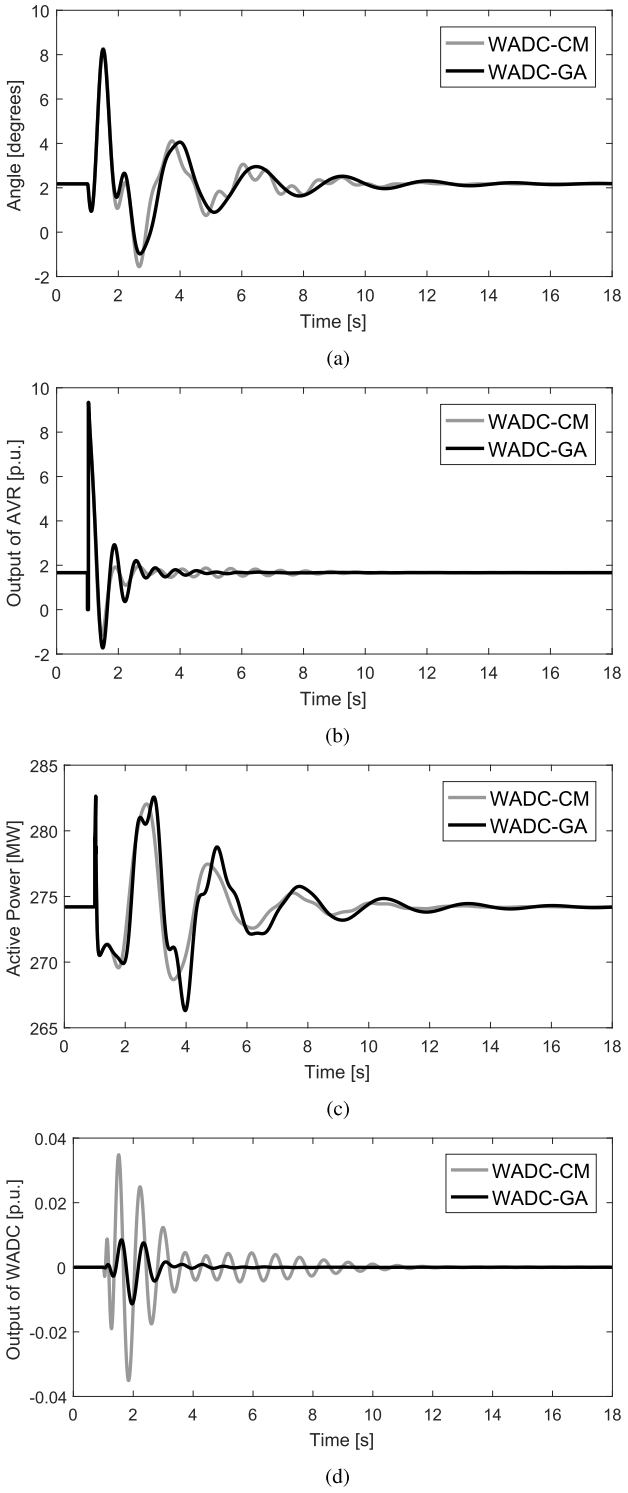

FIGURE 9. Nonlinear simulations for normal operating condition for the worst of C3 case. (a) Angle of the generator 101. (b) Output signal of the AVR of the generator 101. (c) Active power flow in line 506 - 507. (d) Output signal of the WADC for the generator 101.

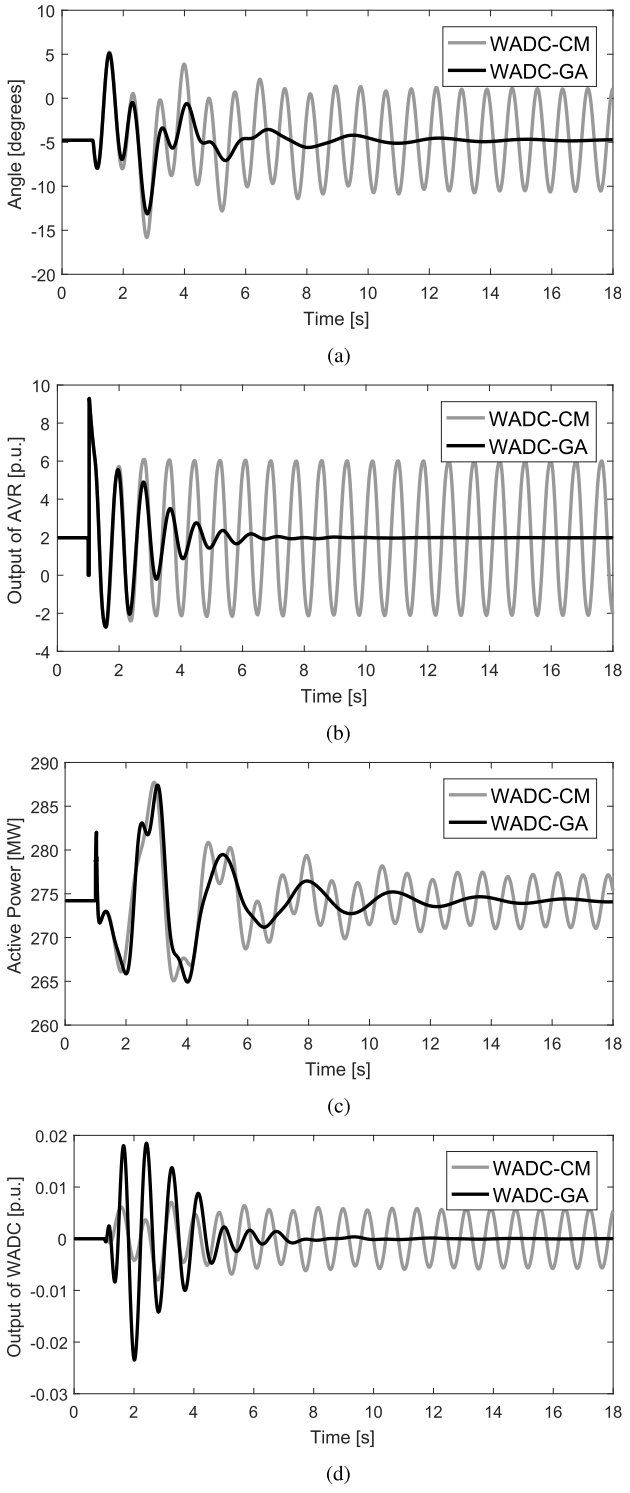

FIGURE 10. Nonlinear simulations for the communication loss of 101 control signal (central controller output) for the worst of C1 case. (a) Angle of the generator 101. (b) Output signal of the AVR of the generator 101. (c) Active power flow in line 506 - 507. (d) Output signal of the WADC for the generator 201.

designed considering the worst operating case for the contingency C1 (Table 2, Row 1). The resulting modal analysis involving all the 198 scenarios for the two-level control is present in Table 3. In this table, only the dominant oscillation mode with the lowest damping ration among these 198 scenarios is shown. In addition, WADC-GA and WADC-CM

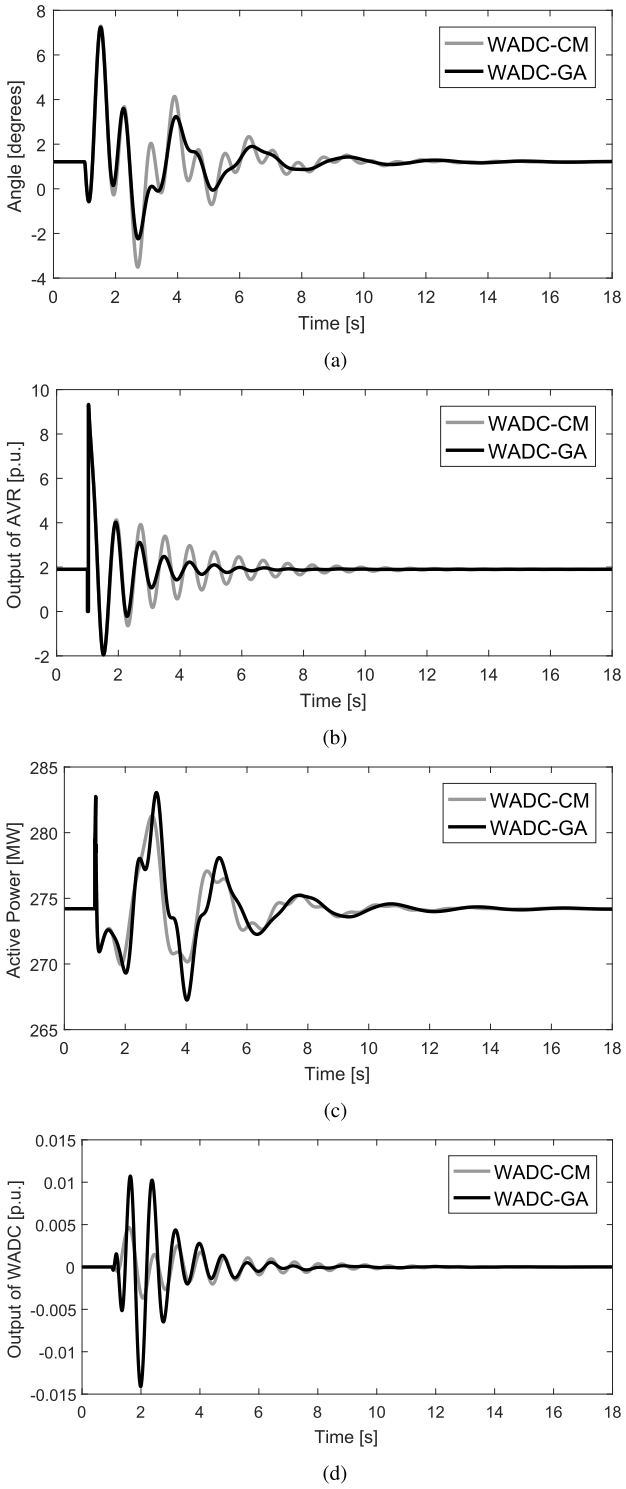

FIGURE 11. Nonlinear simulations for the communication loss of 101 control signal (central controller output) for the worst of C2 case. (a) Angle of the generator 101. (b) Output signal of the AVR of the generator 101. (c) Active power flow in line 506 - 507. (d) Output signal of the WADC for the generator 201.

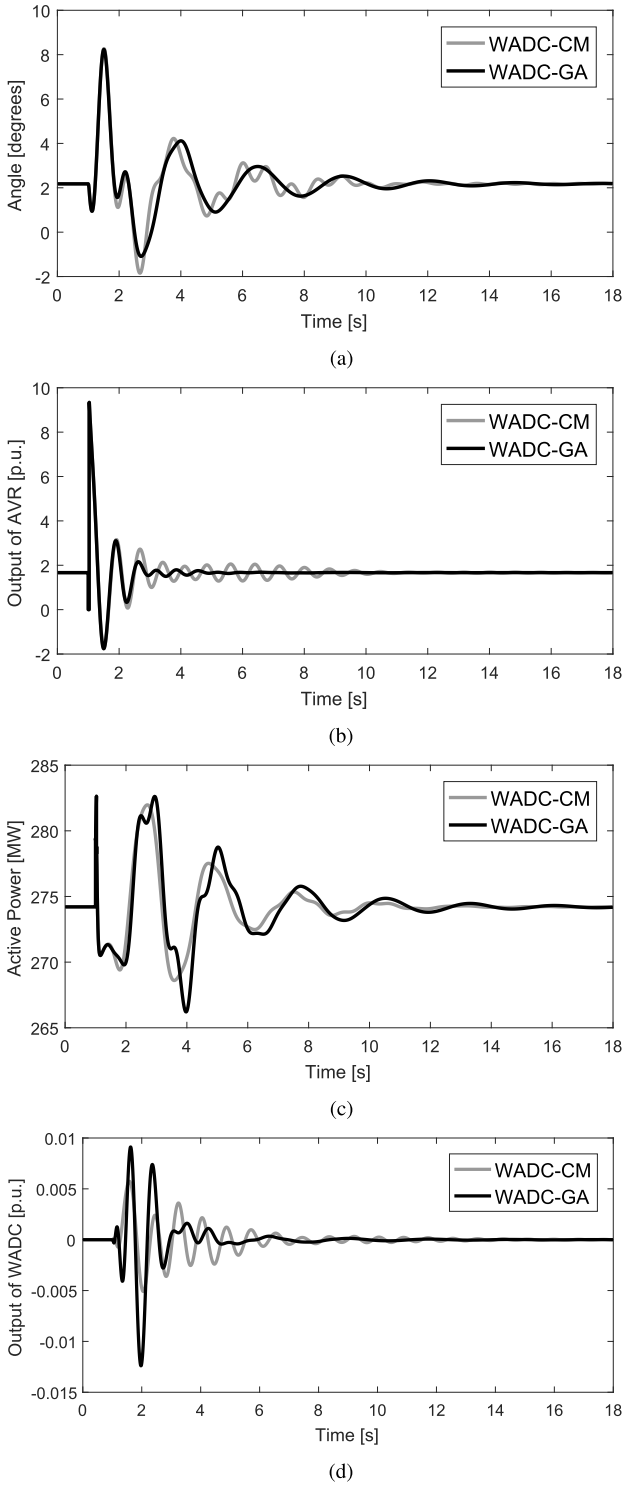

FIGURE 12. Nonlinear simulations for the communication loss of 101 control signal (central controller output) for the worst of C3 case. (a) Angle of the generator 101. (b) Output signal of the AVR of the generator 101. (c) Active power flow in line 506 - 507. (d) Output signal of the WADC for the generator 201.

refer to the centralized controller designed by, respectively, the GA and classical methods.

In order to compare the performance of both controllers (that is, the WADC-GA and WADC-CM) for all the 198 scenarios, Figs. 5 and 6 show the dominant oscillation mode for each of these scenarios in the complex plane. It can be clearly seen that the GA method presents better

TABLE 3. Dominant oscillation modes.

Case	Controller (WADC)	Frequency (Hz)	Damping (%)
The worst of all 198 scenarios	GA	0.80	9.29
	CM	1.21	-1.05

performance when compared with the classical approach. Furthermore, in order to evaluate the robustness, the GA method can provide effective damping regardless load level and topological changes.

TABLE 4. System oscillation modes - communication failure.

Case	Controller (WADC)	Frequency (Hz)	Damping (%)
Worst of C1 - 101o	GA	0.80	9.29
	CM	1.22	-0.71
Worst of C1 - 201i	GA	0.81	9.44
	CM	1.22	1.98

The robustness performance of the communication channels loss is presented in Table 4. The case with the lowest damped dominant oscillation mode among the 6 operating points considering the contingency C1 was adopted (worst of C1 case) for loss of output signals from the central controller (Generator 101 - (101o) and input from the central controller (Generator 201 - (201i) and 6). These cases showed the real advantage of FTC control design. The absence of sensor or/and actuator signals do not damage the power system damping performance.

E. CLOSED-LOOP SYSTEM ROBUST STABILITY EVALUATION

In order to evaluate the robustness of the closed-loop system, the polytopic modeling was used. This polytopic model is composed by a set of N typical operating points (load variation and loss of communication channels) in the form of A_{cl}^{i}, $i = 1, \ldots, N$. These models constitute the vertices of the polytopic set, and the closed-loop systems (16), (17) and (18) will present quadratic stability if we find a unique matrix $\mathbf{P}$ that satisfied the following equations [47]:

$$\mathbf{P} = \mathbf{P}^T > 0 \tag{23}$$

$$(\mathbf{A_{cl}}^{\mathbf{i}})^T \cdot \mathbf{P} + \mathbf{P} \cdot \mathbf{A_{cl}}^{\mathbf{i}} < 0 \tag{24}$$

for $i = 1, \ldots, N$.

Using SeDuMi solver [48], the matrix $\mathbf{P}$ was found satisfying the set of equations (23)-(24).

F. NONLINEAR SIMULATION

Since the control design is based on linear models the resulting controller should be validated using a non-linear model of the system. To reach this goal a time domain simulation was conducted using the ANATEM software from CEPEL [49]. Limits of the AVR-PSS and WADCs outputs were considered. The output limits of the AVRs and PSSs are the ones presented in the benchmark and can be found in [39]. The WADC limits chosen were the same for the output signals of the PSS (-0.1,$+0.1$).

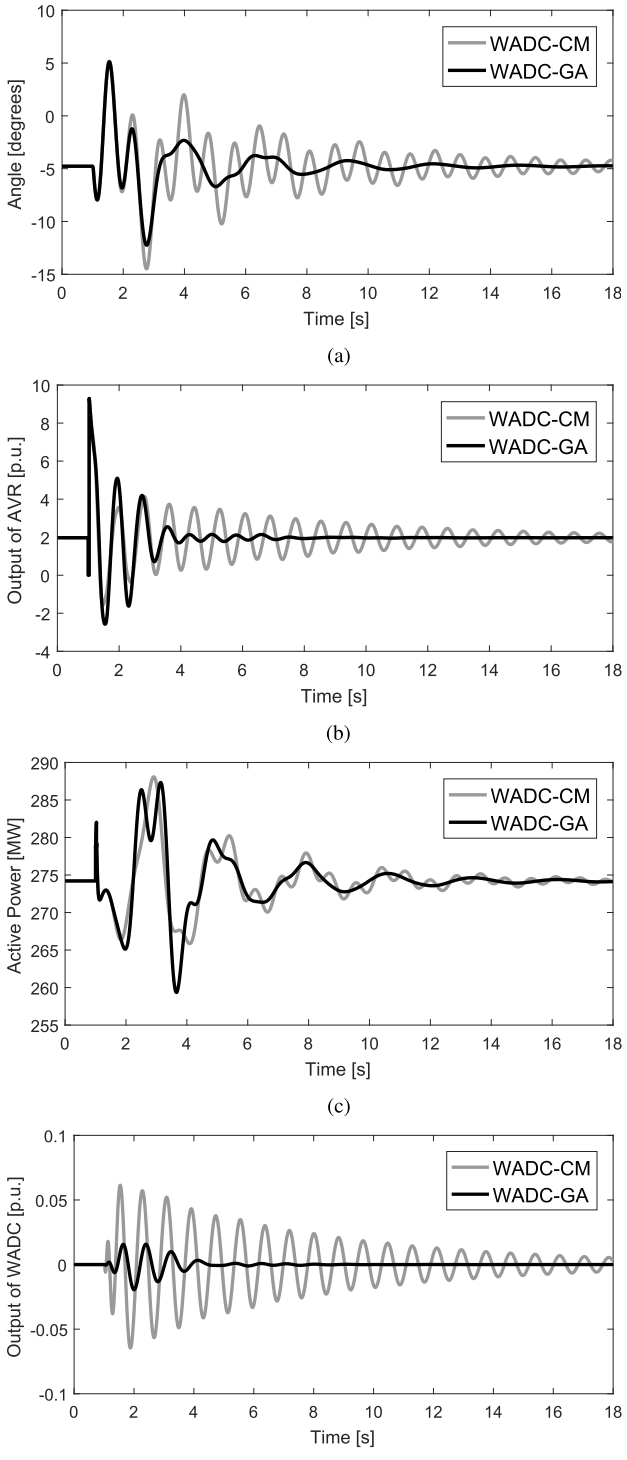

FIGURE 13. Nonlinear simulations for the communication loss of 201 speed signal (central controller input) for the worst of C1 case. (a) Angle of the generator 101. (b) Output signal of the AVR of the generator 101. (c) Active power flow in line 506 - 507. (d) Output signal of the WADC for the generator 101.

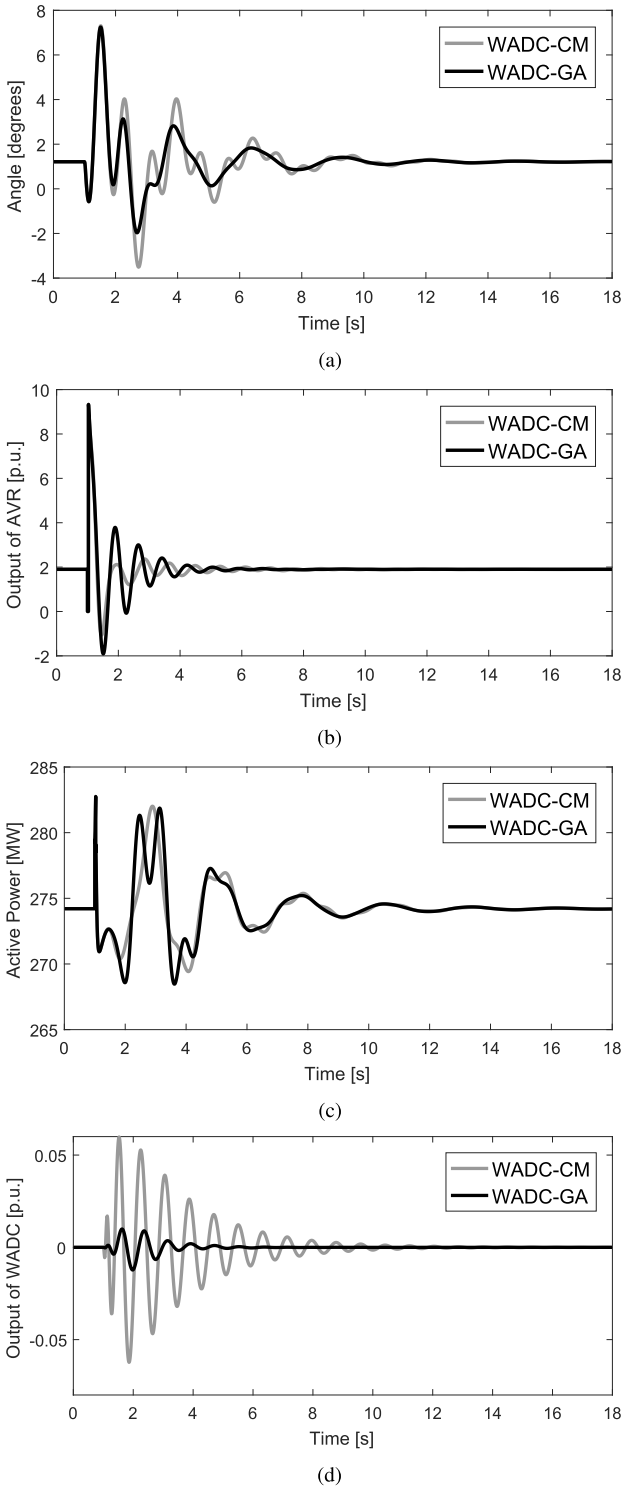

FIGURE 14. Nonlinear simulations for the communication loss of 201 speed signal (central controller input) for the worst of C2 case. (a) Angle of the generator 101. (b) Output signal of the AVR of the generator 101. (c) Active power flow in line 506 - 507. (d) Output signal of the WADC for the generator 101.

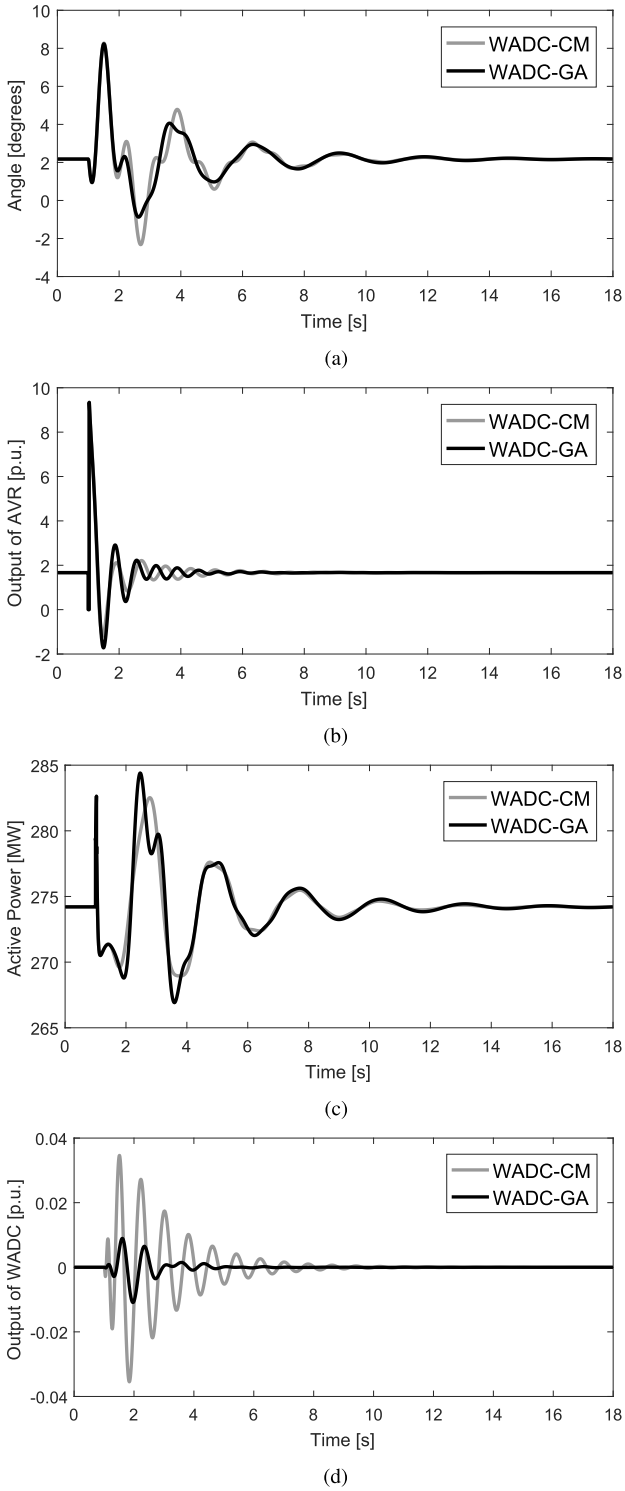

FIGURE 15. Nonlinear simulations for the communication loss of 201 speed signal (central controller input) for the worst of C3 case. (a) Angle of the generator 101. (b) Output signal of the AVR of the generator 101. (c) Active power flow in line 506 - 507. (d) Output signal of the WADC for the generator 101.

1) NORMAL CONDITION

A 30 ms three-phase short-circuit was applied at Bus 101, the worst of C1, C2 and C3 cases, and cleared without any switchings. The curves of the angle of generator 101 and the control effort (field voltage) are shown in Figs. 7(a) and 7(b) for the C1 case, respectively, in

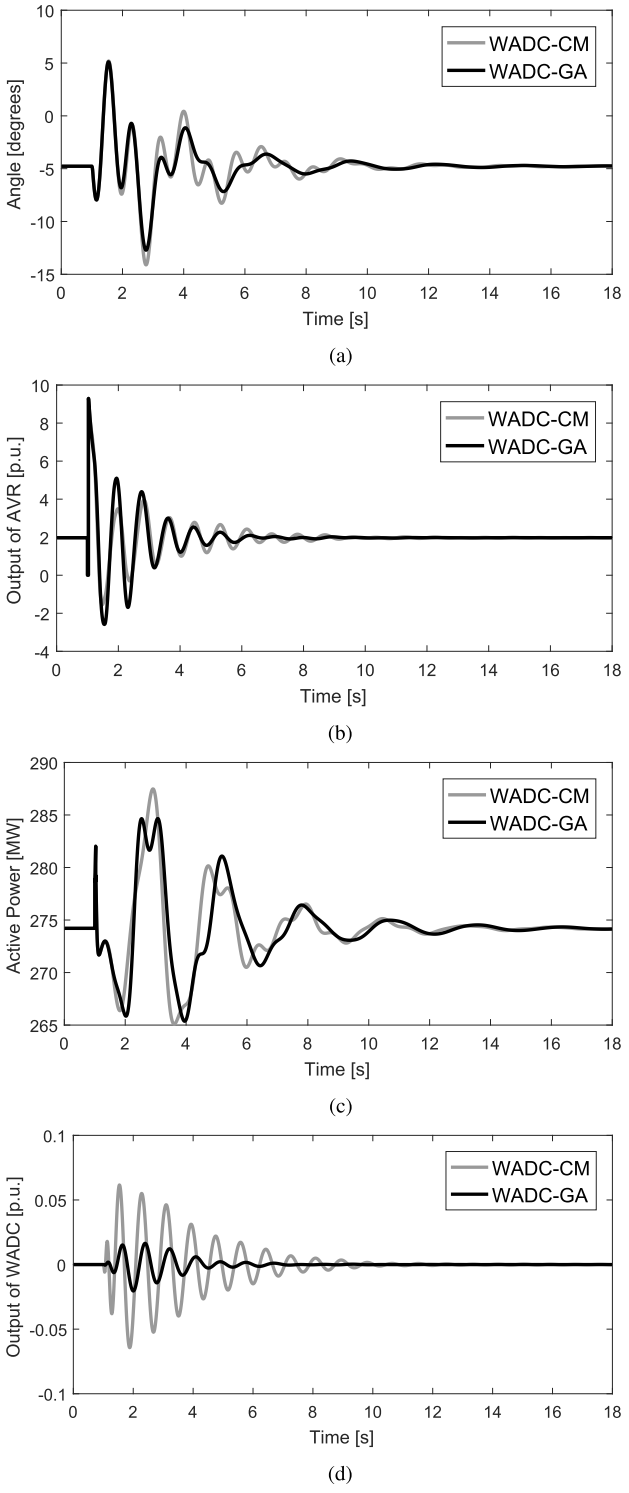

FIGURE 16. Nonlinear simulations for the communication loss of 302 speed signal (central controller input) for the worst of C1 case. (a) Angle of the generator 101. (b) Output signal of the AVR of the generator 101. (c) Active power flow in line 506 - 507. (d) Output signal of the WADC for the generator 101.

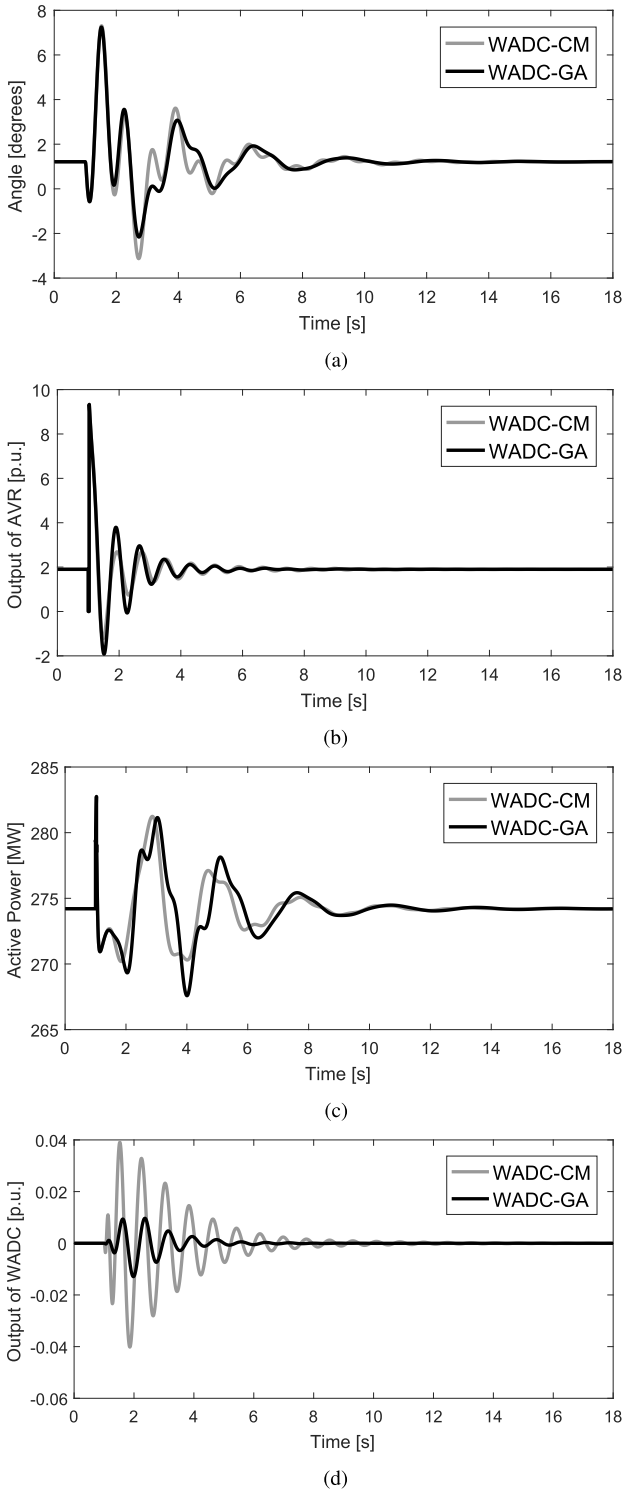

FIGURE 17. Nonlinear simulations for the communication loss of 302 speed signal (central controller input) for the worst of C2 case. (a) Angle of the generator 101. (b) Output signal of the AVR of the generator 101. (c) Active power flow in line 506 - 507. (d) Output signal of the WADC for the generator 101.

Figs. 8(a) and 8(b) for the C2 case and in Figs. 9(a) and 9(b) for the C3 case. The active power flow in the line 506 - 507 for the C1, C2 and C3 cases are shown in Figs. 7(c), 8(c) and 9(c) respectively. Additionally, Figs. 7(d), 8(d) and 9(d) show the output signal of the WADC for the input of the AVR of the generator 101 for the C1, C2 and C3 cases respectively. These figures compare the results from the

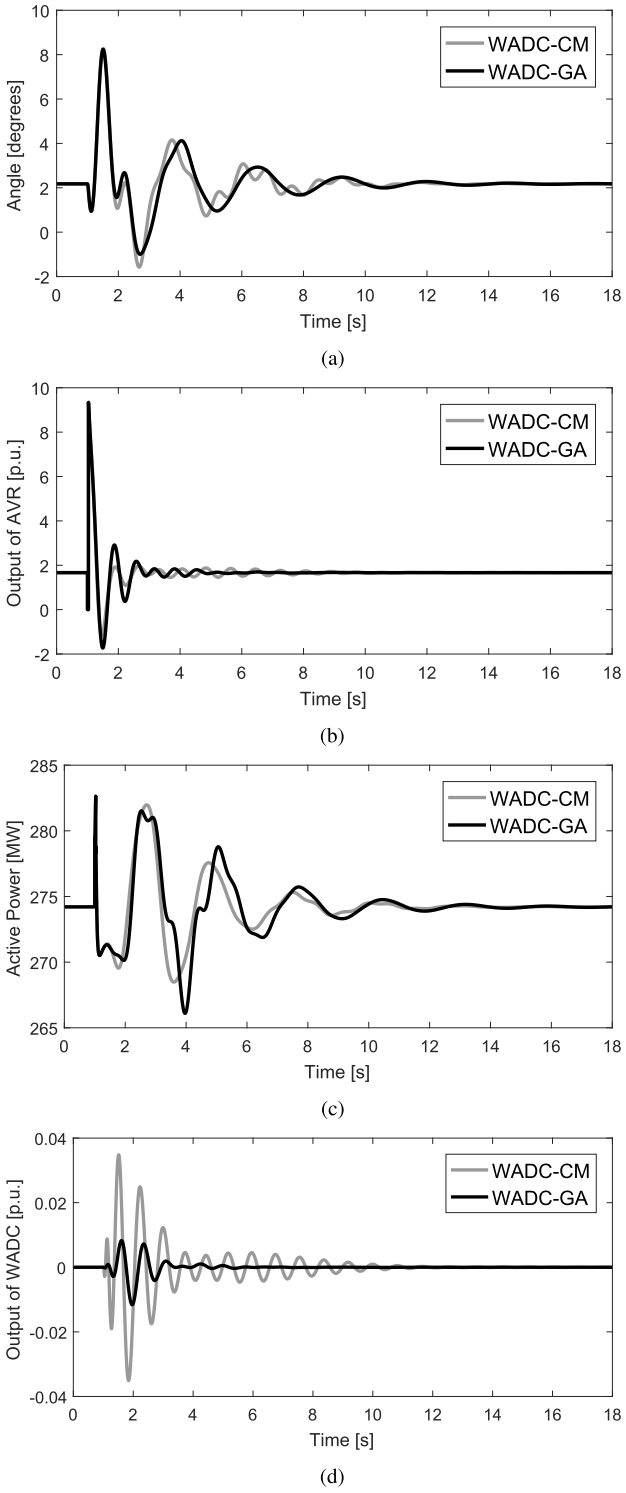

FIGURE 18. Nonlinear simulations for the communication loss of 302 speed signal (central controller input) for the worst of C3 case. (a) Angle of the generator 101. (b) Output signal of the AVR of the generator 101. (c) Active power flow in line 506 - 507. (d) Output signal of the WADC for the generator 101.

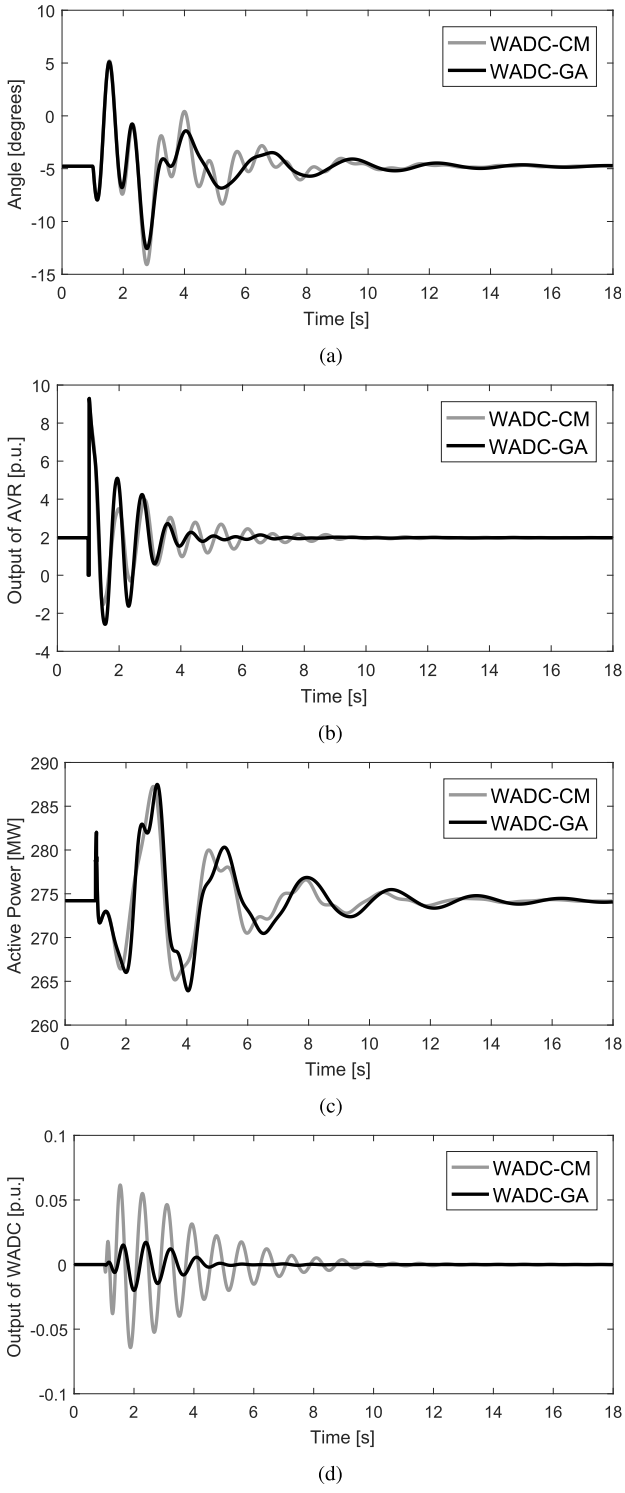

FIGURE 19. Nonlinear simulations for the communication loss of 401 control signal (central controller output) for the worst of C1 case. (a) Angle of the generator 101. (b) Output signal of the AVR of the generator 101. (c) Active power flow in line 506 - 507. (d) Output signal of the WADC for the generator 101.

central controller designed by the classical methodology (WADC-CM) and by the proposed methodology (WADC-GA). Such wide-area stabilizing can be finished in approximately 11s indicating satisfactory control performance. The field voltage responses do not present any limit violation.

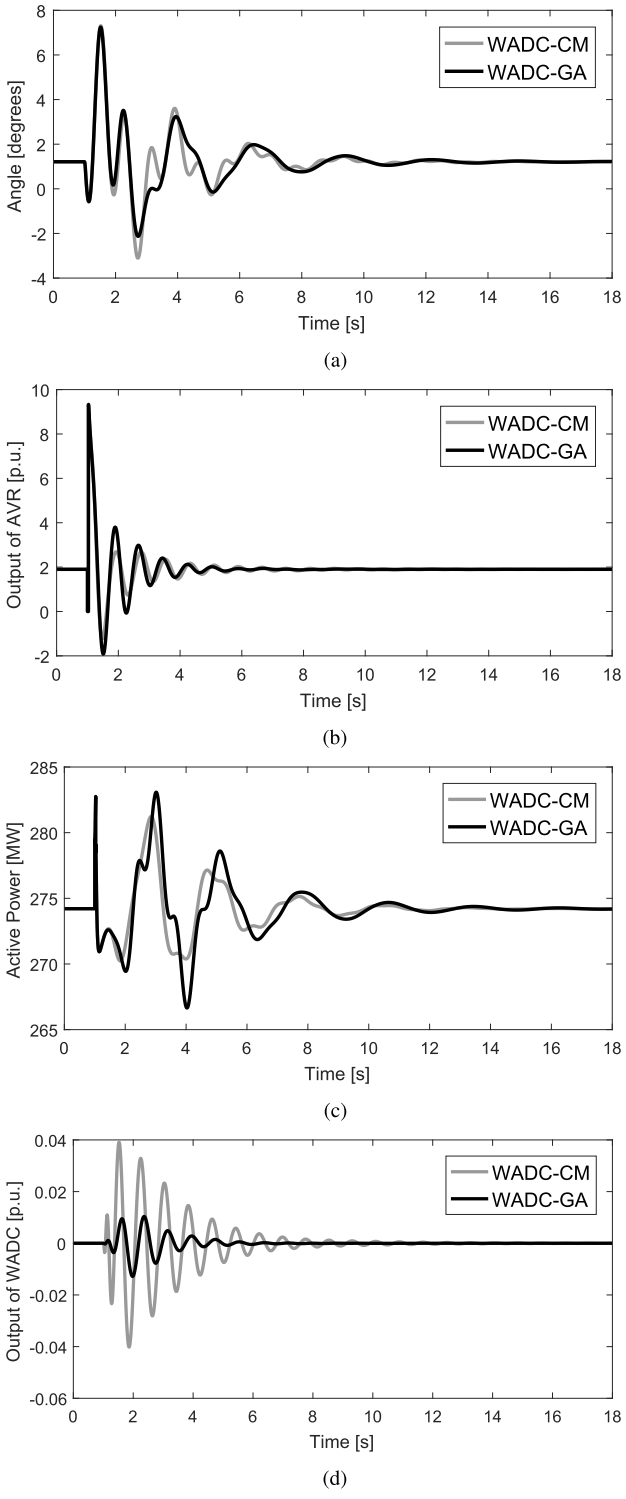

FIGURE 20. Nonlinear simulations for the communication loss of 401 control signal (central controller output) for the worst of C2 case. (a) Angle of the generator 101. (b) Output signal of the AVR of the generator 101. (c) Active power flow in line 506 - 507. (d) Output signal of the WADC for the generator 101.

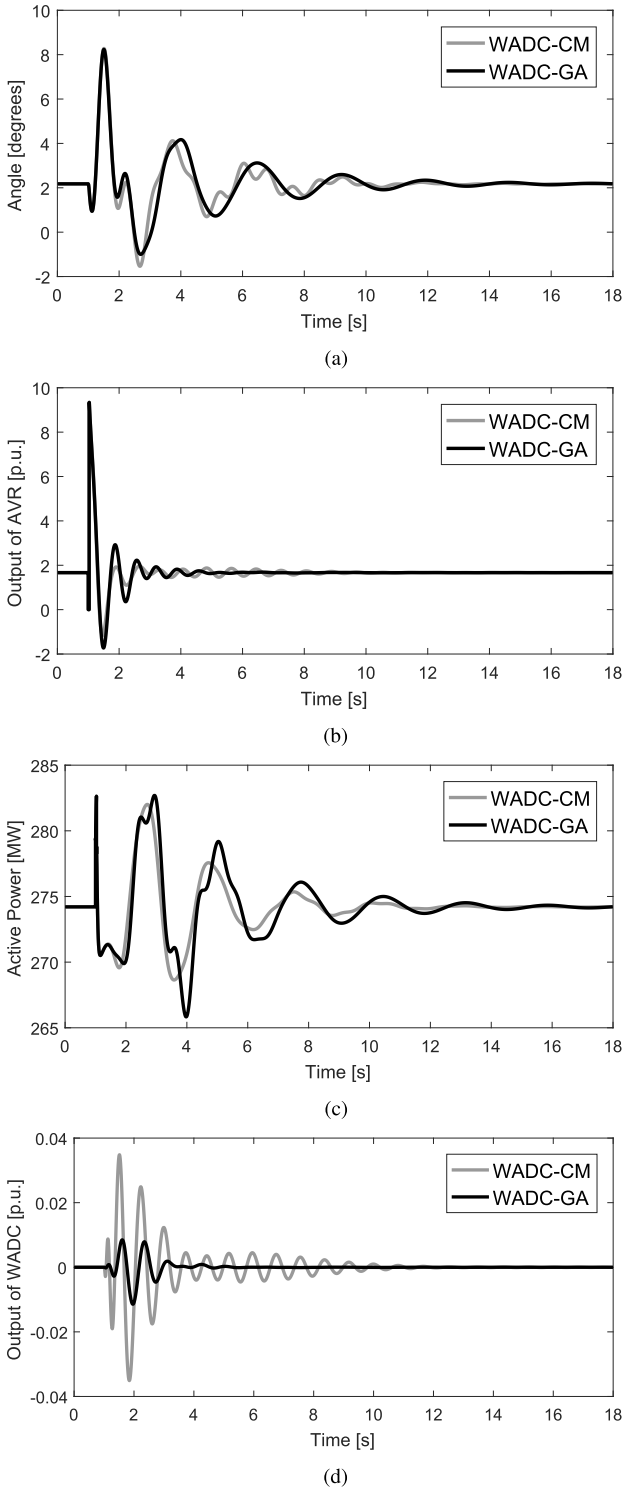

FIGURE 21. Nonlinear simulations for the communication loss of 401 control signal (central controller output) for the worst of C3 case. (a) Angle of the generator 101. (b) Output signal of the AVR of the generator 101. (c) Active power flow in line 506 - 507. (d) Output signal of the WADC for the generator 101.

2) LOSS OF COMMUNICATION CHANNELS

The centralized control depends on the remote signals acquired by the PMUs and the transmission of the control signals to the power plants.

The communication loss of the control signal transmitted to the generator 101 is considered. A 30 ms three-phase short-circuit was applied at Bus 101, worst of C1, C2 and C3 cases, and cleared without any switchings. The angle of

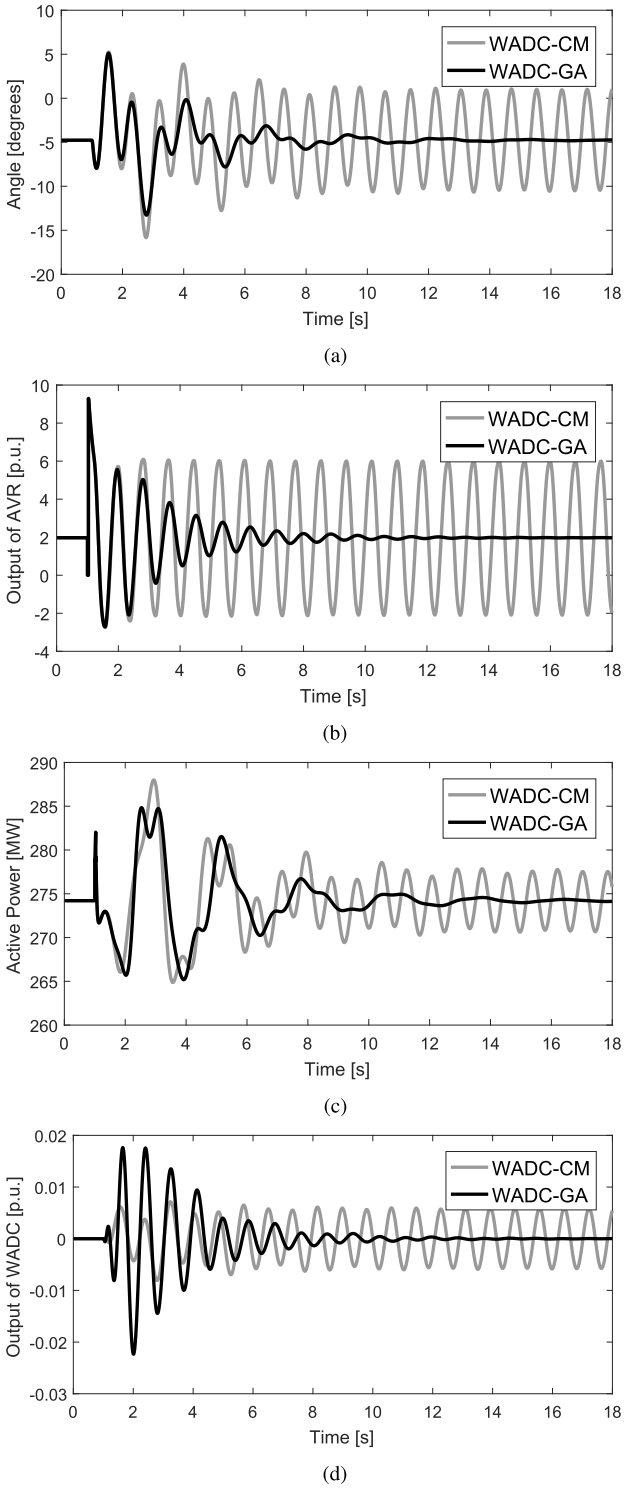

FIGURE 22. Nonlinear simulations for the communication losses of 101 control signal (central controller output) and 302 speed signal (central controller input) for the worst of C1 case. (a) Angle of the generator 101. (b) Output signal of the AVR of the generator 101. (c) Active power flow in line 506 - 507. (d) Output signal of the WADC for the generator 201.

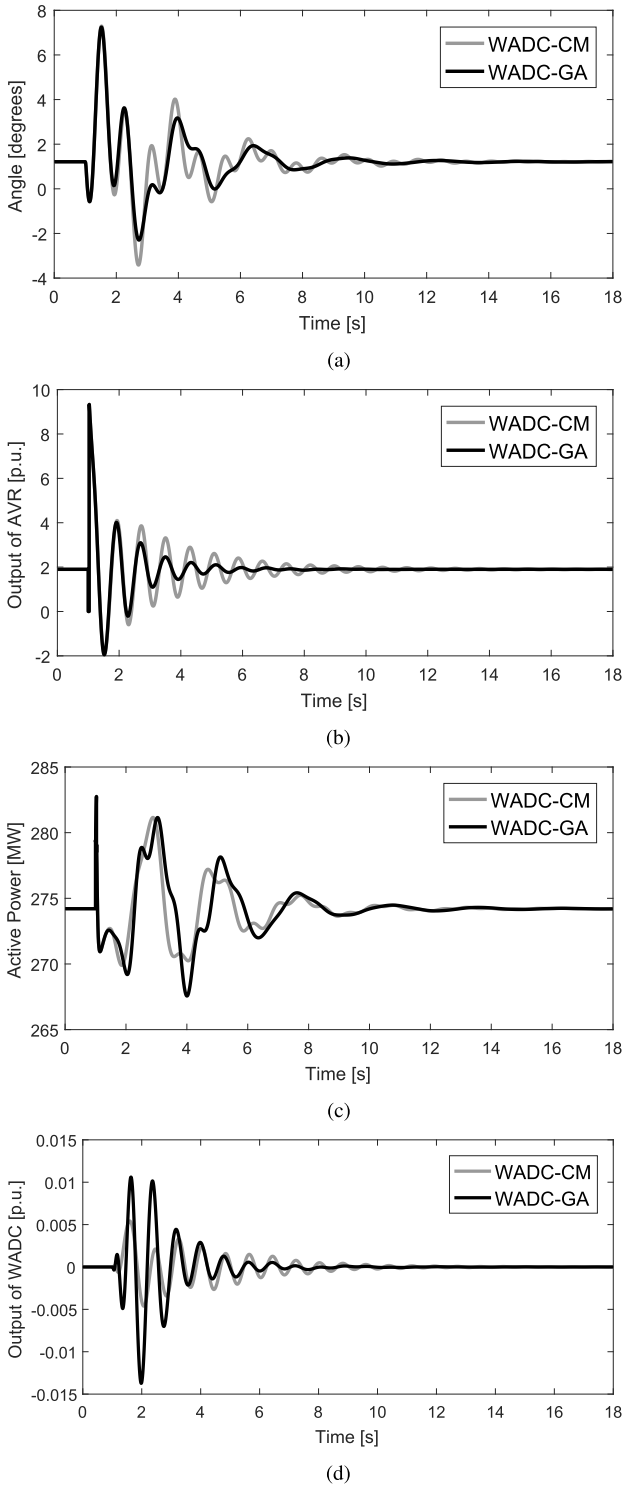

FIGURE 23. Nonlinear simulations for the communication losses of 101 control signal (central controller output) and 302 speed signal (central controller input) for the worst of C2 case. (a) Angle of the generator 101. (b) Output signal of the AVR of the generator 101. (c) Active power flow in line 506 - 507. (d) Output signal of the WADC.

Generator 101 and field voltage (control effort) are shown in Figs. 10(a) and 10(b), respectively for the worst of C1 case and Figs. 11(a) and 11(b) for the worst of C2 case and Figs. 12(a) and 11(b) for the worst of C3 case. The active power flow in the line 506 - 507 for the worst of C1, C2 and C3 cases are shown in Fig. 10(c), Fig. 11(c) and Fig. 12(c), respectively. Additionally, Figs. 10(d), 11(d) and 12(d)

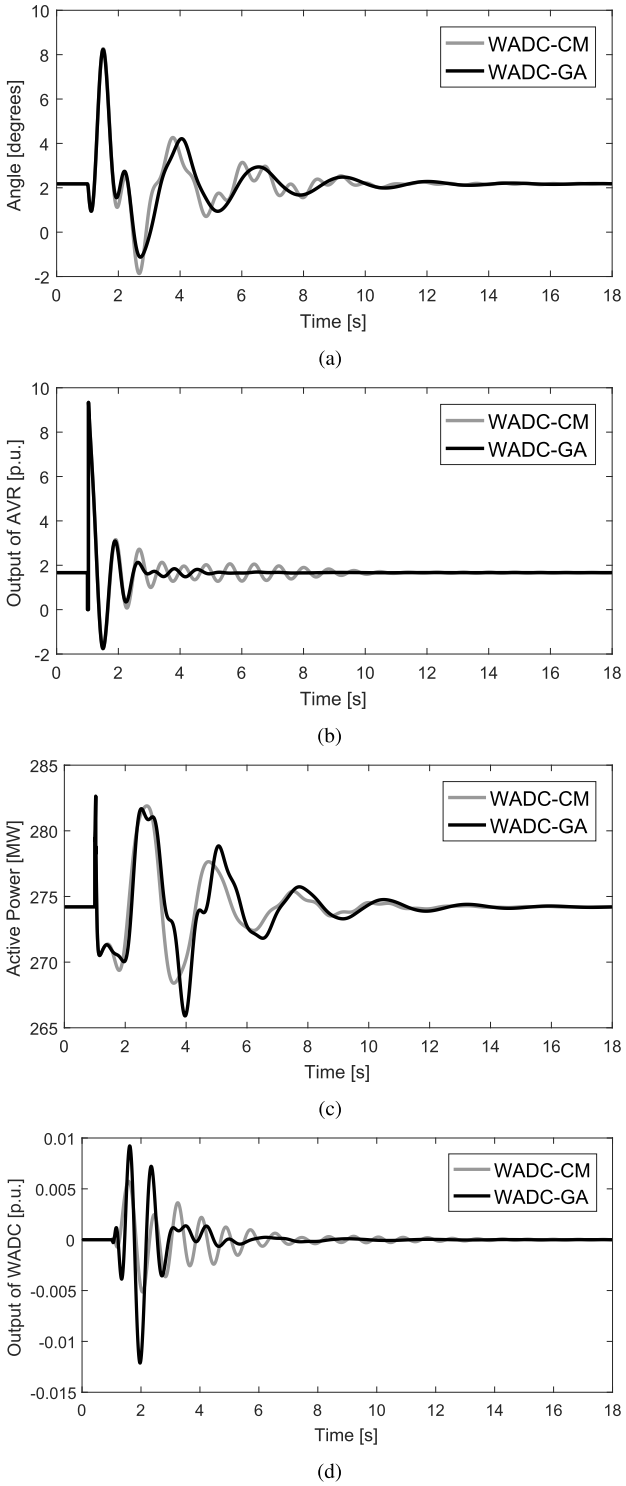

FIGURE 24. Nonlinear simulations for the communication losses of 101 control signal (central controller output) and 302 speed signal (central controller input) for the worst of C3 case. (a) Angle of the generator 101. (b) Output signal of the AVR of the generator 101. (c) Active power flow in line 506 - 507. (d) Output signal of the WADC for the generator 201.

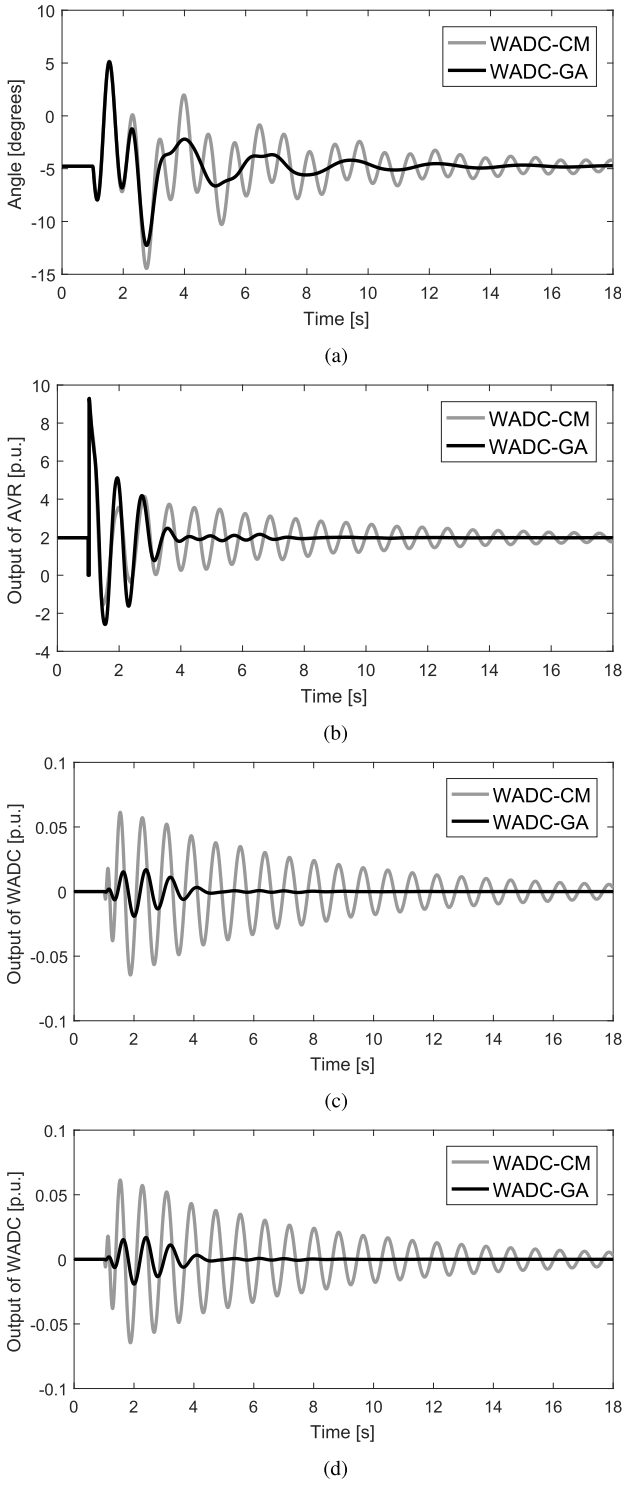

FIGURE 25. Nonlinear simulations for the communication losses of 201 and 401 speed signals (central controller inputs) for the worst of C1 case. (a) Angle of the generator 101. (b) Output signal of the AVR of the generator 101. (c) Active power flow in line 506 - 507. (d) Output signal of the WADC for the generator 101.

show the output signal of the WADC for the input of the AVR of the generator 201 for the C1, C2 and C3 cases respectively.

Looking at this, it is visible to verify the improved performance of FTC controller. Despite the loss of communication channel, the power system response is not degraded.

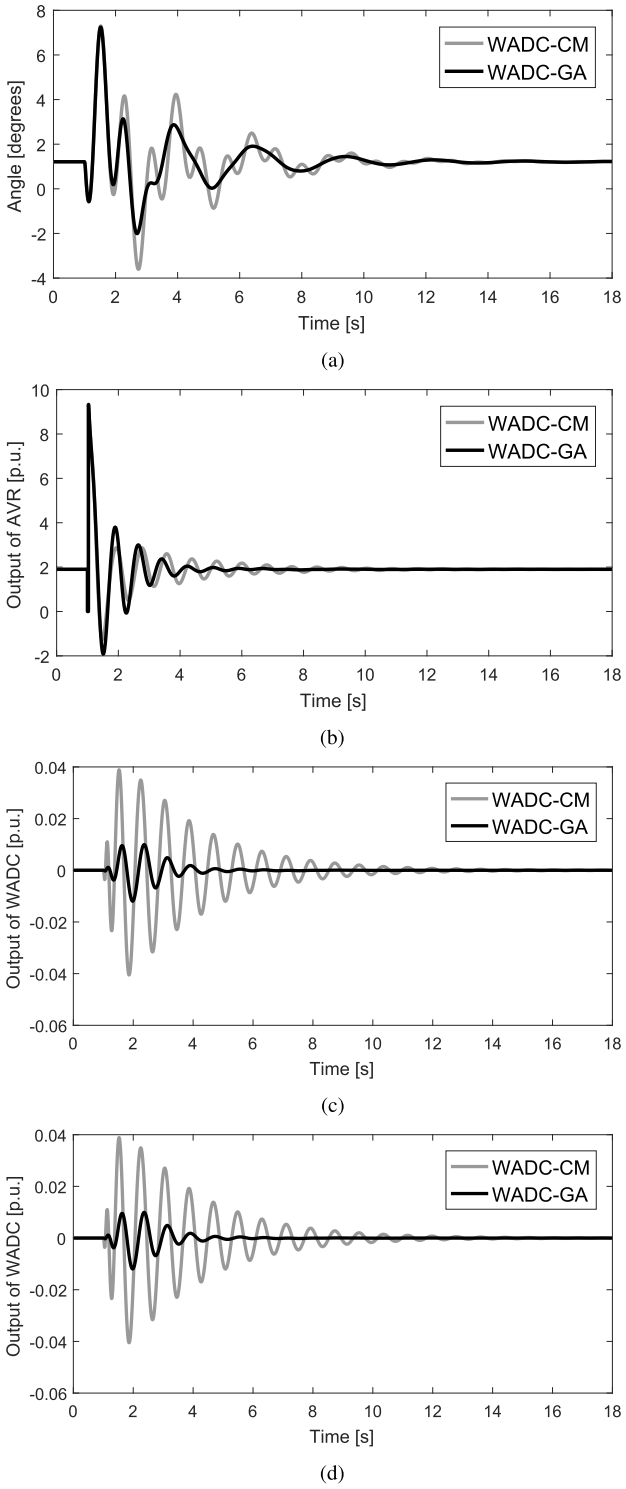

FIGURE 26. Nonlinear simulations for the communication losses of 201 and 401 speed signals (central controller inputs) for the worst of C2 case. (a) Angle of the generator 101. (b) Output signal of the AVR of the generator 101. (c) Active power flow in line 506 - 507. (d) Output signal of the WADC for the generator 101.

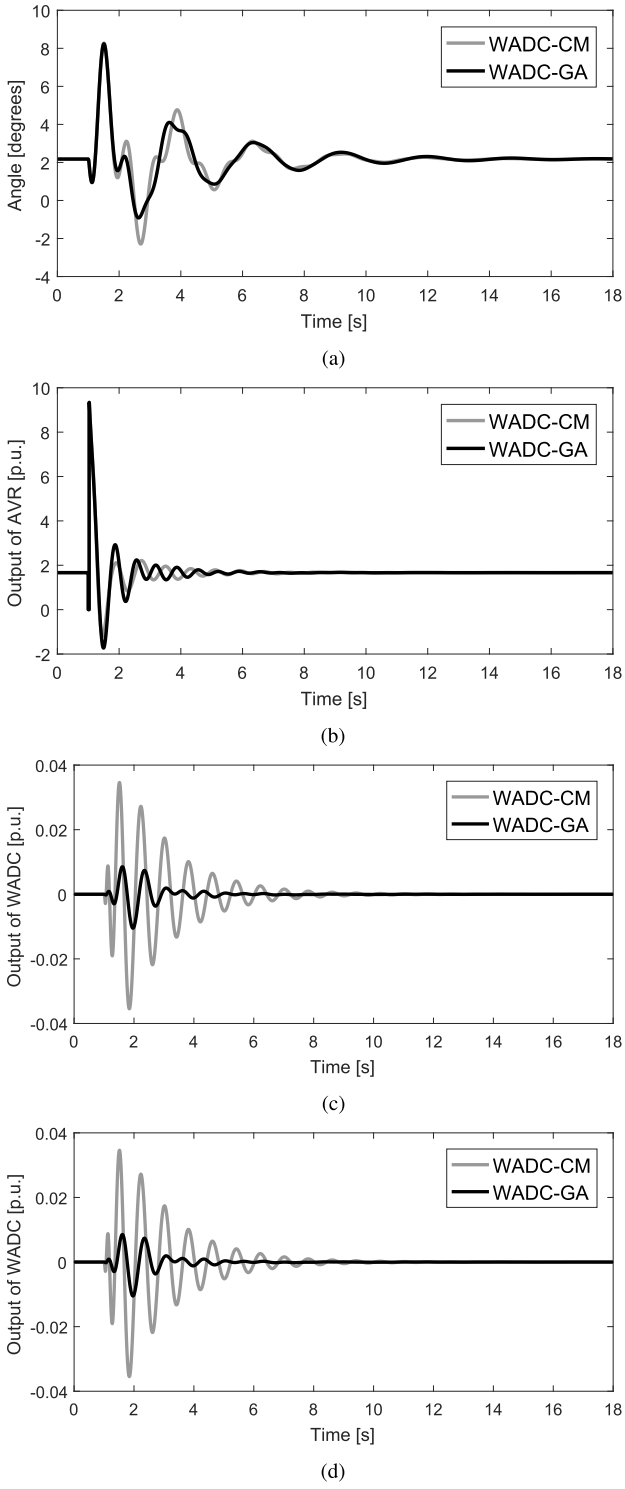

FIGURE 27. Nonlinear simulations for the communication losses of 201 and 401 speed signals (central controller inputs) for the worst of C3 case. (a) Angle of the generator 101. (b) Output signal of the AVR of the generator 101. (c) Active power flow in line 506 - 507. (d) Output signal of the WADC for the generator 101.

The control effort does not violate any limits and keep the damping performance as expected.

Additionally, the communication loss of 201 speed signal (central controller input) was also considered. A 30 ms three-phase short-circuit was applied at Bus 101, worst of C1, C2 and C3 cases, and cleared without any switchings. The angle of generator 101 and field voltage (control effort) for

the worst of C1 are shown in Figs. 13(a) and 13(b), respectively, for the worst of C2 are shown in Figs. 14(a) and 14(b), respectively, and for the worst of C3 are shown in Figs. 15(a) and 15(b), respectively. The active power flow in the line 506 - 507 for the worst of C1, C2 and C3 cases are shown in Figs. 13(c), 14(c) and 15(c), respectively. Additionally, Figs. 13(d), 14(d) and 15(d) show the output signal of the WADC for the input of the AVR of the generator 101 for the C1, C2 and C3 cases respectively. The same analysis was carried out for the communication loss of 302 speed and loss of 401 control signals and the results are presented in Figs. (16(a)-18(d)), and Figs. (19(a)-21(d)), respectively. Once again, the angular response presents a satisfactory power system damping response showing the main advantage of FTC controller. The control effort does not violate the actuator limits.

3) MORE THAN ONE COMMUNICATION CHANNEL LOSS

In order to evaluate when more than one communication loss occurs, this section presents results of two simultaneous communication losses. Figures 22(a), 22(b) and 22(c) presents the angle and field voltage of the generator 101 and active power flow in line 506 - 507 when the central controller output 101 and input 302 are permanent lost for the worst of C1 case. Figures 23(a), 23(b) and 23(c) presents the angle and field voltage of the generator 101 and active power flow in line 506 - 507 when the central controller output 101 and input 302 are permanent lost for the worst of C2 case. Besides, Figures 24(a), 24(b) and 24(c) presents the angle and field voltage of the generator 101 and active power flow in line 506 - 507 when the central controller output 101 and input 302 are permanent lost for the worst of C3 case. Additionally, Figs. 22(d), 23(d) and 24(d) show the output signal of the WADC for the input of the AVR of the generator 201 for the worst of C1, C2 and C3 cases respectively.

Figures 25(a), 25(b) and 25(c) presents the angle and field voltage of the generator 101 and active power flow in line 506 - 507 when the central controller inputs 201 and 401 are permanent lost for the worst of C1 case. Figures 26(a), 26(b) and 26(c) presents the angle and field voltage of the generator 101 and active power flow in line 506 - 507 when the central controller inputs 201 and 401 are permanent lost for the worst of C2 case. Besides, Figures 27(a), 27(b) and 27(c) presents the angle and field voltage of the generator 101 and active power flow in line 506 - 507 when the central controller inputs 201 and 401 are permanent lost for the worst of C3 case. Additionally, Figs. 25(d), 26(d) and 27(d) show the output signal of the WADC for the input of the AVR of the generator 101 for the worst of C1, C2 and C3 cases respectively.

In both cases, the dynamic response of the system with WADC-GA presented a satisfactory dynamic performance even when two signal simultaneous losses occur.

VI. CONCLUSIONS

This research presented a design procedure, which may be used as a guideline, for a passive FTC two-level controller. To the best of our knowledge, this is the first work considering a two-level controller with multiple inputs-outputs and fixed-order controller design.

This control design method fulfills all requirements necessary for practical wide-area power damping controllers. The two main advantages, for this critical power system application, are the robustness to communication channel failures (which may be due to cyber-attacks, for example) and easy application. In other words, actuators and/or sensor failures do not undermine the power system dynamical response. The method also allows the inclusion of communication delays in the design. Additionally, the control design method is validated by simulation for several operating conditions, and this allows reducing the need of PSS retuning or diagnoses for pre-specified contingencies.

Test results in the Simplified 14-Generator Model of the Southeastern Australian Power System have shown the

$$CC_{GA}(s) = \begin{bmatrix} \frac{11.1s^2-10.8s+11.6}{s^2+7.31s+5.86} & \frac{0.8s^2-9.6s+2.0}{s^2+7.31s+5.86} & \frac{1.9s^2+9.3s+11.8}{s^2+7.31s+5.86} & \frac{8.1s^2-9.3s-14.5}{s^2+7.31s+5.86} & \frac{1.2s^2-5.9s-0.4}{s^2+7.31s+5.86} \\ \frac{12.9s^2-6.6s+8.6}{s^2+7.31s+5.86} & \frac{-1.9s^2-9.2s-0.04}{s^2+7.31s+5.86} & \frac{-4.6s^2-3.1s+1.8}{s^2+7.31s+5.86} & \frac{3.5s^2-14.8s+12.6}{s^2+7.31s+5.86} & \frac{1.1s^2-12.2s-13.4}{s^2+7.31s+5.86} \\ \frac{-1.2s^2-13.6s+13.0}{s^2+7.31s+5.86} & \frac{s^2-14.4s-13.2}{s^2+7.31s+5.86} & \frac{12s^2+1.6s+10.1}{s^2+7.31s+5.86} & \frac{-8.5s^2+1.7s-1.6}{s^2+7.31s+5.86} & \frac{3.7s^2-12.4s-13.4}{s^2+7.31s+5.86} \\ \frac{-3.5s^2+6.1s+4.9}{s^2+7.31s+5.86} & \frac{-1.8s^2+2.5s+8.9}{s^2+7.31s+5.86} & \frac{-12.7s^2-13s+4.6}{s^2+7.31s+5.86} & \frac{-10s^2+11.9s-12.3}{s^2+7.31s+5.86} & \frac{7.4s^2+12.5s+6.1}{s^2+7.31s+5.86} \\ \frac{-7.5s^2-3.6s+11.4}{s^2+7.31s+5.86} & \frac{11.6s^2+13.7s+8.7}{s^2+7.31s+5.86} & \frac{-13.1s^2-3.2s+9.1}{s^2+7.31s+5.86} & \frac{4.8s^2-12.7s-5.6}{s^2+7.31s+5.86} & \frac{-9.6s^2-9.2s+1.2}{s^2+7.31s+5.86} \end{bmatrix} \quad (25)$$

$$CC_{CM}(s) = \begin{bmatrix} \frac{260s^2+1277s+1568}{s^2+48.58+590.1} & \frac{s^2+11.49s+33}{s^2+20.77s+107.8} & \frac{s^2+6.44s+10.37}{s^2+37.05s+343.2} & \frac{s^2+6.44s+10.37}{s^2+37.05s+343.2} & \frac{10s^2+72.03s+129.7}{s^2+33.12s+274.3} \\ \frac{s^2+7.203s+12.97}{s^2+33.12s+274.3} & \frac{11.7s^2+162.8s+566.1}{s^2+17.15s+73.53} & \frac{s^2+7.203s+12.97}{s^2+33.12s+274.3} & \frac{0.1s^2+2.666s+17.77}{s^2+8.949s+20.02} & \frac{s^2+7.866s+15.47}{s^2+30.33s+230} \\ \frac{s^2+9.036s+20.41}{s^2+26.4s+174.3} & \frac{s^2+4.363s+4.76}{s^2+54.68s+747.5} & \frac{s^2+15.47s+59.81}{s^2+15.43s+59.48} & \frac{s^2+14.4s+51.87}{s^2+16.56s+68.59} & \frac{0.1s^2+3.751s+35.17}{s^2+6.361s+10.12} \\ \frac{s^2+7.07s+12.5}{s^2+33.75s+284.7} & \frac{s^2+7.646s+14.62}{s^2+31.2s+243.2} & \frac{s^2+3.002s+2.254}{s^2+79.47s+1579} & \frac{20s^2+173.7s+377}{s^2+27.48s+188.7} & \frac{s^2+4.679s+5.474}{s^2+50.99s+650} \\ \frac{s^2+13.9s+48.29}{s^2+17.17s+73.67} & \frac{s^2+9.185s+21.09}{s^2+25.97s+168.7} & \frac{s^2+16.51s+68.17}{s^2+14.45s+52.19} & \frac{s^2+9.618s+23.12}{s^2+24.81s+153.9} & \frac{30s^2+240.9s+483.5}{s^2+29.72s+220.7} \end{bmatrix} \quad (26)$$

effectiveness of the control scheme. The controller performance was also validated by non-linear simulation and compared with a design method largely used in the power industry. The potential of the proposed design method for power system damping opens the opportunity to explore this control design technique for other critical problems in the power system area such as transient stability closed-loop emergency control and small-signal damping performance of systems with large penetration of renewable energy sources.

APPENDIX
WIDE-AREA DAMPING CONTROLLERS

The central controllers designed for the Simplified 14-Generator Model of the Southeastern Australian Power System using the Proposed Approach and Classical Method are presented in (25) and (26), as shown at the bottom of the previous page, respectively.

REFERENCES

[1] P. Kundur, "Definition and classification of power system stability IEEE/CIGRE joint task force on stability terms and definitions," *IEEE Trans. Power Syst.*, vol. 19, no. 3, pp. 1387–1401, May 2004.
[2] D. Trudnowski, D. Kosterev, and J. Undrill, "PDCI damping control analysis for the western North American power system," in *Proc. IEEE Power Energy Soc. General Meeting (PES)*, Jul. 2013, pp. 1–5.
[3] P. Overholt, D. Ortiz, and A. Silverstein, "Synchrophasor technology and the DOE: Exciting opportunities lie ahead in development and deployment," *IEEE Power Energy Mag.*, vol. 13, no. 5, pp. 14–17, Sep./Oct. 2015.
[4] J. Yang, Y. Yu, and B. Chen, "The smart grids in China—A review," *Energies*, vol. 5, no. 12, pp. 1321–1338, 2012.
[5] M. Zima, M. Larsson, P. Korba, C. Rehtanz, and G. Andersson, "Design aspects for wide-area monitoring and control systems," *Proc. IEEE*, vol. 93, no. 5, pp. 980–996, May 2005.
[6] V. Terzija *et al.*, "Wide-area monitoring, protection, and control of future electric power networks," *Proc. IEEE*, vol. 99, no. 1, pp. 80–93, Jan. 2011.
[7] J. H. Chow, J. J. Sanchez-Gasca, H. Ren, and S. Wang, "Power system damping controller design-using multiple input signals," *IEEE Control Syst.*, vol. 20, no. 4, pp. 82–90, Aug. 2000.
[8] I. Kamwa, R. Grondin, and Y. Hebert, "Wide-area measurement based stabilizing control of large power systems—A decentralized/hierarchical approach," *IEEE Trans. Power Syst.*, vol. 16, no. 1, pp. 136–153, Feb. 2001.
[9] V. A. F. De Campos and J. J. da Cruz, "Robust hierarchized controllers using wide area measurements in power systems," *Int. J. Elect. Power Energy Syst.*, vol. 83, pp. 392–401, Dec. 2016.
[10] W. Yao, L. Jiang, Q. H. Wu, J. Y. Wen, and S. J. Cheng, "Delay-dependent stability analysis of the power system with a wide-area damping controller embedded," *IEEE Trans. Power Syst.*, vol. 26, no. 1, pp. 233–240, Feb. 2011.
[11] L. Cheng, G. Chen, W. Gao, F. Zhang, and G. Li, "Adaptive time delay compensator (ATDC) design for wide-area power system stabilizer," *IEEE Trans. Smart Grid*, vol. 5, no. 6, pp. 2957–2966, Nov. 2014.
[12] W. Yao, L. Jiang, J. Wen, Q. H. Wu, and S. Cheng, "Wide-area damping controller of FACTS devices for inter-area oscillations considering communication time delays," *IEEE Trans. Power Syst.*, vol. 29, no. 1, pp. 318–329, Jan. 2014.
[13] W. Yao, L. Jiang, J. Wen, Q. Wu, and S. Cheng, "Wide-area damping controller for power system interarea oscillations: A networked predictive control approach," *IEEE Trans. Control Syst. Technol.*, vol. 23, no. 1, pp. 27–36, Jan. 2015.
[14] Y. Yuan, Y. Sun, and L. Cheng, "Design of delayed-input wide-area FACTS controller using genetic algorithm," in *Proc. IEEE Power Eng. Soc. Gen. Meeting*, Jun. 2007, pp. 1–6.
[15] Y. Shen, W. Yao, J. Wen, and H. He, "Adaptive wide-area power oscillation damper design for photovoltaic plant considering delay compensation," *IET Generat., Transmiss. Distrib.*, vol. 11, no. 18, pp. 4511–4519, Dec. 2017.
[16] D. Dotta, A. S. E. Silva, and I. C. Decker, "Wide-area measurements-based two-level control design considering signal transmission delay," *IEEE Trans. Power Syst.*, vol. 24, no. 1, pp. 208–216, Feb. 2009.
[17] S. Zhang and V. Vittal, "Wide-area control resiliency using redundant communication paths," *IEEE Trans. Power Syst.*, vol. 29, no. 5, pp. 2189–2199, Sep. 2014.
[18] Y. Shen, W. Yao, J. Wen, H. He, and L. Jiang, "Resilient wide-area damping control using GrHDP to tolerate communication failures," *IEEE Trans. Smart Grid*, to be published, doi: 10.1109/TSG.2018.2803822.
[19] S. Sheng, W. L. Chan, K. K. Li, D. Xianzhong, and Z. Xiangjun, "Context information-based cyber security defense of protection system," *IEEE Trans. Power Del.*, vol. 22, no. 3, pp. 1477–1481, Jul. 2007.
[20] A. Hahn and M. Govindarasu, "Cyber attack exposure evaluation framework for the smart grid," *IEEE Trans. Smart Grid*, vol. 2, no. 4, pp. 835–843, Dec. 2011.
[21] D. Wei, Y. Lu, M. Jafari, P. M. Skare, and K. Rohde, "Protecting smart grid automation systems against cyberattacks," *IEEE Trans. Smart Grid*, vol. 2, no. 4, pp. 782–795, Dec. 2011.
[22] A. Hahn, A. Ashok, S. Sridhar, and M. Govindarasu, "Cyber-physical security testbeds: Architecture, application, and evaluation for smart grid," *IEEE Trans. Smart Grid*, vol. 4, no. 2, pp. 847–855, Jun. 2013.
[23] R. Liu, C. Vellaithurai, S. S. Biswas, T. T. Gamage, and A. K. Srivastava, "Analyzing the cyber-physical impact of cyber events on the power grid," *IEEE Trans. Smart Grid*, vol. 6, no. 5, pp. 2444–2453, Sep. 2015.
[24] S. Mousavian, J. Valenzuela, and J. Wang, "A probabilistic risk mitigation model for cyber-attacks to PMU networks," *IEEE Trans. Power Syst.*, vol. 30, no. 1, pp. 156–165, Jan. 2015.
[25] S. Sojoudi, J. Lavaei, and R. M. Murray, "Fault-tolerant controller design with applications in power systems and synthetic biology," in *Proc. Amer. Control Conf*, Jun. 2011, pp. 4135–4142.
[26] S. Simani, S. Alvisi, and M. Venturini, "Fault tolerant control of a simulated hydroelectric system," *Control Eng. Pract.*, vol. 51, pp. 13–25, Jun. 2016.
[27] M. Staroswiecki, D. Berdjag, B. Jiang, and K. Zhang, "PACT : A passive/active approach to fault tolerant stability under actuator outages," in *Proc. 48h IEEE Conf. Decision Control (CDC) Held Jointly 28th Chin. Control Conf.*, Dec. 2009, pp. 7819–7824.
[28] A. S. Pedersen, J. H. Richter, M. Tabatabaeipour, and H. Jöhannsson, and M. Blanke, "Fault tolerant emergency control to preserve power system stability," *Control Eng. Pract.*, vol. 53, pp. 151–159, Aug. 2016.
[29] S. Zhang and V. Vittal, "Design of wide-area power system damping controllers resilient to communication failures," *IEEE Trans. Power Syst.*, vol. 28, no. 4, pp. 4292–4300, Nov. 2013.
[30] F. R. S. Sevilla, I. Jaimoukha, B. Chaudhuri, and P. Korba, "Fault-tolerant control design to enhance damping of inter-area oscillations in power grids," *Int. J. Robust Nonlinear Control*, vol. 24, nos. 8–9, pp. 1304–1316, May 2014.
[31] A. L. B. D. Bomfim, G. N. Taranto, and D. M. Falcao, "Simultaneous tuning of power system damping controllers using genetic algorithms," *IEEE Trans. Power Syst.*, vol. 15, no. 1, pp. 163–169, Feb. 2000.
[32] E. Alfaro-Cid, E. McGookin, and D. Murray-Smith, "A comparative study of genetic operators for controller parameter optimisation," *Control Eng. Pract.*, vol. 17, no. 1, pp. 185–197, Jan. 2009.
[33] M. F. Castoldi, D. S. Sanches, M. R. Mansour, N. G. Bretas, and R. A. Ramos, "A hybrid algorithm to tune power oscillation dampers for FACTS devices in power systems," *Control Eng. Pract.*, vol. 24, pp. 25–32, Mar. 2014.
[34] M. E. C. Bento, D. Dotta, and R. A. Ramos, "Performance analysis of wide-area damping control design methods," in *Proc. IEEE Power Energy Soc. Gen. Meet.*, Jul. 2016, pp. 1–5.
[35] *IEEE Recommended Practice for Excitation System Models for Power System Stability Studies*, Standard, Apr. 2006.
[36] M. Vajta, "Some remarks on Padé-approximations," in *Proc. 3rd TEMPUS-INTCOM Symp.*, Veszprém, Hungary, Sep. 2005, vol. 19. no. 3, pp. 1387–1401.
[37] P. Kundur, *Power System Stability and Control*. New York, NY, USA: McGraw-Hill, 1994.
[38] S. Gomes, N. Martins, and C. Portela, "Computing small-signal stability boundaries for large-scale power systems," *IEEE Trans. Power Syst.*, vol. 18, no. 2, pp. 747–752, May 2003.
[39] R. A. Ramos *et al.*, "Benchmark systems for small-signal stability analysis and control," PES Resour. Center, Tech. Rep., Aug. 2015. [Online]. Available: http://resourcecenter.ieee-pes.org/pes/product/technical-reports/PESTR18

[40] C. Canizares *et al.*, "Benchmark models for the analysis and control of small-signal oscillatory dynamics in power systems," *IEEE Trans. Power Syst.*, vol. 32, no. 1, pp. 715–722, Jan. 2017.
[41] B. Pal and B. Chaudhuri, *Robust Control in Power Systems*. Boston, MA, USA: Springer, 2005, doi: 10.1007/b136490.
[42] S. Furuya and J. Irisawa, "A robust H_∞ power system stabilizer design using reduced-order models," *Int. J. Elect. Power Energy Syst.*, vol. 28, no. 1, pp. 21–28, Jan. 2006.
[43] R. A. Jabr, B. C. Pal, and N. Martins, "A sequential conic programming approach for the coordinated and robust design of power system stabilizers," *IEEE Trans. Power Syst.*, vol. 25, no. 3, pp. 1627–1637, Aug. 2010.
[44] M. E. C. Bento, D. Dotta, R. Kuiava, and R. A. Ramos, "Design of coordinated decentralized damping controllers for power systems considering uncertainties," *J. Control, Autom. Elect. Syst.*, vol. 29, no. 1, pp. 22–31, Feb. 2018, doi: 10.1007/s40313-017-0351-x.
[45] E. V. Larsen and D. A. Swann, "Applying power system stabilizers part II: Performance objectives and tuning concepts," *IEEE Trans. Power App. Syst.*, vol. PAS-100, no. 6, pp. 3025–3033, Jun. 1981.
[46] P. Kundur, M. Klein, G. J. Rogers, and M. S. Zywno, "Application of power system stabilizers for enhancement of overall system stability," *IEEE Trans. Power Syst.*, vol. 4, no. 2, pp. 614–626, May 1989.
[47] R. A. Ramos, L. F. C. Alberto, and N. G. Bretas, "A new methodology for the coordinated design of robust decentralized power system damping controllers," *IEEE Trans. Power Syst.*, vol. 19, no. 1, pp. 444–454, Feb. 2004.
[48] J. F. Sturm, "Using SeDuMi 1.02, a MATLAB toolbox for optimization over symmetric cones," *Optim. Methods Softw.*, vol. 11, nos. 1–4, pp. 625–653, 1999.
[49] CEPEL. (2014). *Anatem User's Manual Version 10.5.2*. [Online]. Available: http://www.dre.cepel.br/

MURILO E. C. BENTO (S'14) received the B.Sc. and M.Sc. degrees in electrical engineering from the University of São Paulo, São Carlos, Brazil, in 2013 and 2016, respectively.

He is currently pursuing the Ph.D. degree with the Department of Electrical Engineering, Engineering School, University of São Paulo. His research interests include power system stability analysis and control, with emphasis on small-signal and voltage stability problems.

DANIEL DOTTA (M'18) received the B.S., M.S., and Ph.D. degrees from UFSC, Florianópolis, Brazil. He was with the Federal Institute of Santa Catarina. He joined the University of Campinas in 2015, where he is currently an Assistant Professor. He also spent his sabbatical leave as a Visiting Scholar with the Rensselaer Polytechnic Institute, Troy, NY, USA, from 2012 to 2013.

ROMAN KUIAVA (S'05–M'10) received the M.Sc. and Ph.D. degrees in electrical engineering from the University of São Paulo, São Carlos, Brazil, in 2007 and 2010, respectively.

He is currently an Adjunct Professor with the Department of Electrical Engineering, Polytechnic Center, Federal University of Paraná, Curitiba, Brazil. His research interests include power system stability analysis and control, with emphasis on transient and small-signal stability problems.

RODRIGO A. RAMOS (S'97–M'03–SM'08) received the M.Sc. and Ph.D. degrees in electrical engineering from the University of São Paulo, São Carlos, Brazil, in 1999 and 2002, respectively.

He was a Visiting Associate Professor with the University of Waterloo, Canada, in 2013, and a Visiting Fellow with the University of New South Wales, Australia, in 2008. He is currently an Associate Professor with the Department of Electrical Engineering, Engineering School, University of São Paulo. His research interests include power system stability analysis and control, with emphasis on small-signal and voltage stability problems.